

American University in Cairo

## AUC Knowledge Fountain

---

Theses and Dissertations

Student Research


---

Summer 6-15-2021

### On-Chip Nanoscale Plasmonic Optical Modulators

Abdallahman Mohamed Nader Abdelhamid  
abdallahman.nader@aucegypt.edu

Follow this and additional works at: <https://fount.aucegypt.edu/etds>

 Part of the [Electrical and Electronics Commons](#), [Electromagnetics and Photonics Commons](#), [Electronic Devices and Semiconductor Manufacturing Commons](#), and the [Optics Commons](#)

---

#### Recommended Citation

##### APA Citation

Abdelhamid, A. M. (2021). *On-Chip Nanoscale Plasmonic Optical Modulators* [Master's Thesis, the American University in Cairo]. AUC Knowledge Fountain.

<https://fount.aucegypt.edu/etds/1602>

##### MLA Citation

Abdelhamid, Abdallahman Mohamed Nader. *On-Chip Nanoscale Plasmonic Optical Modulators*. 2021. American University in Cairo, Master's Thesis. *AUC Knowledge Fountain*.

<https://fount.aucegypt.edu/etds/1602>

This Master's Thesis is brought to you for free and open access by the Student Research at AUC Knowledge Fountain. It has been accepted for inclusion in Theses and Dissertations by an authorized administrator of AUC Knowledge Fountain. For more information, please contact [mark.muehlhaeusler@aucegypt.edu](mailto:mark.muehlhaeusler@aucegypt.edu).

**The American University in Cairo**  
**School of Sciences and Engineering**

# **On-Chip nanoscale plasmonic optical modulators**

**A Thesis submitted to**

**Physics Program**

**In partial fulfillment of the requirements for**

**The Degree of Master of Science in Physics**

**Submitted by: Abdalrahman Mohamed Nader**

**Date: 2<sup>nd</sup> of February 2021**

# Acknowledgment

First and before all, I have to thank God. Then I express my sincere thanks to my supervisor, Dr. Mohamed Swillam, for the research guidance and the patience over the whole master's period, and for letting me be a part of the Nano-Photonics Research Lab (NRL) in the American University in Cairo. I would like to extend my thanks to members of the NRL, for their help and friendship that will definitely continue for several years. I would like to thank Eng. Hany for setting up and support in the computer labs.

I would like to acknowledge the American University in Cairo for providing me a fellowship to fund this Master of Science degree. I would like to especially thank the course instructors: Dr. Salah El Nahewy, Dr. Mohamed El Fiky, Dr. Yehia Ismail. Every course increased my interest and passion in physics.

Lumerical is acknowledged for providing licenses for their software.

I would like to thank my parents and my brother for their continuous support, my beloved wife, Rana, for her presence and encouragement. At last I have to thank a lot of friends, current ones, and old ones, specially Mohamed Elsayed, Ragi Samir, Ahmed Bassam and Omar Sherif, I also would like to thank, Mohamed Salah and Mahmoud Seddik for their help and friendship in the physics labs.

# Abstract

In this thesis work, techniques for downsizing Optical modulators to nanoscale for the purpose of utilization in on chip communication and sensing applications are explored. Nanoscale optical interconnects can solve the electronics speed limiting transmission lines, in addition to decrease the electronic chips heat dissipation. A major obstacle in the path of achieving this goal is to build optical modulators, which transforms data from the electrical form to the optical form, in a size comparable to the size of the electronics components, while also having low insertion loss, high extinction ratio and bandwidth. Also, lap-on-chip applications used for fast diagnostics, and which is based on photonic sensors and photonic circuitry, is in need for similar modulator specifications, while it loosens the spec on the modulator's size.

Silicon photonics is the most convenient photonics technology available for optical interconnects application, owing to its compatibility with the mature and cheap CMOS manufacturing process. Hence, building modulators which is exclusively compatible with this technology is a must, although, Plasmonics could be the right technology for downsizing the optical components, owing to its capability in squeezing light in subwavelength dimensions. Hence, our major goal is to build plasmonic modulators, that can be coupled directly to silicon waveguides. A Plasmonic Mach-Zehnder modulator was built, based on the orthogonal junction coupling technique. The footprint of the modulator is decreased to  $0.6\mu\text{m} \times 4.7\mu\text{m}$ , extinction ratio of 15.8 dB and insertion loss of 3.38 dB at 10 volts was achieved in the 3D simulations. The voltage length product for the modulator is  $47 \text{ V}\mu\text{m}$ . The orthogonal junction coupler technique minimized the modulator's footprint.

On the other hand, photonic sensors favorably work in the mid-infrared region, owing to the presence of a lot of molecules absorption peaks in this region. Hence, III-V semiconductor media is used for this type of applications, owing to the availability of laser sources built of III-V media, and to the lower losses that these materials have in mid-infrared region. Hybrid plasmonic waveguide, formed of doped InAs, AlAs and GaAs is studied extensively. Based on this waveguide an electro-absorption modulator is built. The device showed an extinction ratio of 15 dB at  $40\mu\text{m}$  length, and 2 dB of insertion loss. The small device footprint predicts a much lower energy consumption.

# Table of Contents

Acknowledgment .....	2
Abstract.....	3
Table of Contents.....	4
Chapter 1 : Introduction .....	11
1.1 Optical Modulators .....	11
1.2 Modulators Classification.....	12
1.3 Plasmon Polaritons .....	12
1.4 On Chip Modulators.....	13
1.5 Objectives and scope of thesis.....	14
1.6 References .....	16
Chapter 2 : Background and Literature review.....	18
2.1 Silicon Optical Modulators.....	18
2.2 Plasmonic modulators.....	21
2.3 Midinfrared Modulators .....	22
References .....	23
Chapter 3 : Electro-Optic Plasmonic Modulator with Direct Coupling to Silicon Waveguides ....	27
Abstract:.....	27
Introduction .....	27

3.1	Operation principle .....	28
3.2	Our Novel Designs.....	30
3.3	Modulator characteristics.....	32
3.4	Conclusion.....	35
	References .....	36
Chapter 4 : Negative & Positive dispersion engineering in mid- infrared region for hybrid plasmonic waveguide.....		
		39
	Abstract.....	39
	Introduction .....	39
4.1	Overview and Material Modeling .....	40
4.2	Results & discussion.....	43
4.3	Conclusion:.....	50
	References .....	50
Chapter 5 : Mid-infrared III-V Electro-Absorption Hybrid Plasmonic Modulator.....		
		52
5.1	Introduction .....	52
5.2	Modulator Principle .....	54
5.3	Charge Simulations .....	55
5.4	Modal Analysis: .....	61
5.5	FDTD Simulations .....	65
5.6	Conclusion.....	69

References: .....	69
Chapter 6 : Conclusion .....	71
Bibliography .....	73
6.1 .....	73

**List of figures**

Figure 1-1 silicon based photonic circuit [1].....	11
Figure 1-2, Surface plasmon polaritons .....	13
Figure 2-1 Proposed SOI p+-n-n+ channel-waveguide electro-optical phase modulator18. [10] .....	19
Figure 2-2 Three-terminal modulator proposed by [12]. .....	20
Figure 2-3 The figure shows the switching energy vs operating frequency of different types of optical modulators.....	22
Figure 3-1 The MZM, with input and output silicon waveguides, the modulator arms are plasmonic slot waveguides filled with nonlinear polymer, with two silver triangles at the input and output. The x-y plane contains the top plane of the modulator. ....	29
Figure 3-2 The z-component of the magnetic field (Hz) at wavelength equals to 1.55 $\mu$ m for the On state of the modulator (a), and the Off state (b).....	29

Figure 3-3 The transmission (output power/input power) of the modulator versus the width of the silicon waveguide (Si WG) at a height equal to 340 nm, and wavelength equal to 1.55  $\mu\text{m}$  at zero voltage (On state). ..... 31

Figure 3-4 The transmission (output power/input power) in the On and Off states. The blue solid is for the 10V modulator whose length is 4.7  $\mu\text{m}$ . The red dashed is for the 6V modulator whose length is 8.1  $\mu\text{m}$ . ..... 33

Figure 3-5 The two curves show the normalized coupling in any of the two arm, in the on (solid green) and off (dashed red) states. Both are for the 10V modulator (the legend is for both graphs).35

Figure 4-1 the hybrid plasmonic waveguide, labeled with the materials used, symbols for dimensions and the axes direction and position..... 41

Figure 4-2 shows the real and imaginary parts of the refractive index (upper curve). shows the real and imaginary parts of the relative permittivity (lower curve). ..... 43

Figure 4-3 fig(3a) shows the surface plot and 1D plot of the modal shape at wavelength equals 3.3  $\mu\text{m}$ , fig(3b) at wavelength equals 8  $\mu\text{m}$ , and fig(3c) shows a dispersion curve, all are at doping =  $2.5\text{E}20 \text{ cm}^{-3}$ ,  $W = 2 \mu\text{m}$ ,  $H = 0.6 \mu\text{m}$ , and  $h = 100 \text{ nm}$ . The 1D plots are taken at the white dashed lines in the surface plot..... 44

Figure 4-4 Modal shapes taken at the dashed white line in the above surface plot..... 44

Figure 4-5 The modal shapes of the plasmonic modes at different doping, all are at wavelength = 7.5  $\mu\text{m}$   $W = 2\mu\text{m}$ ,  $H = 0.3\mu\text{m}$ . ..... 45

Figure 4-6 shows the modal shapes at different dimensions. fig(6a) is at doping equals  $2.5\text{E}20 \text{ cm}^{-3}$ , wavelength equals 7  $\mu\text{m}$ , fig(6b) is at doping equals  $5\text{E}19 \text{ cm}^{-3}$ , wavelength equals 8  $\mu\text{m}$ , fig(6c) is at doping equals  $7.5\text{E}19 \text{ cm}^{-3}$ , wavelength equals 7  $\mu\text{m}$ , fig(6d) is at doping equals  $1\text{E}20 \text{ cm}^{-3}$ , wavelength equals 7  $\mu\text{m}$ . ..... 45

Figure 4-7 The effective mode index ( $n_{\text{eff}}$ ) and the extension coefficient ( $k$ ) at various doping ( $2.5\text{E}20 \text{ cm}^{-3}$ ,  $1\text{E}20 \text{ cm}^{-3}$ ,  $7.5\text{E}19 \text{ cm}^{-3}$ ,  $5\text{E}19 \text{ cm}^{-3}$ ). The vertical dashed lines mark the position of



the plasma wavelength, the green line, the red, and the cyan line are for  $1E20 \text{ cm}^{-3}$ ,  $7.5E19 \text{ cm}^{-3}$ ,  $5E19 \text{ cm}^{-3}$  doping respectively. The plasma wavelength of the  $2.5E20 \text{ cm}^{-3}$  is below  $3 \text{ }\mu\text{m}$ . ..... 46

Figure 4-8 shows dispersion curves at doping levels, and different widths and heights, for the waveguide, at constant core height, which is equal to  $100 \text{ nm}$ . ..... 48

Figure 4-9 shows dispersion curves at different core heights ( $h$ ), at different doping levels, all the curves are at waveguide width equal to  $2 \text{ }\mu\text{m}$ , and height equal to  $0.6 \text{ }\mu\text{m}$ . ..... 49

Figure 5-1, to the left (a), the hybrid plasmonic waveguide built on a GaAs substrate is shown. To the right (b), the modulator schematic shows the mode coupling from the GaAs/AlGaAs optical waveguide to the hybrid plasmonic waveguide, and then back to the optical wave guide..... 54

Figure 5-2, the modulator design showing the GaAs substrate, the AlGaAs buffer layer, then the GaAs rip waveguide, then the Hybrid plasmonic AlAs and doped InAs layers, and the Aluminum contacts for electrical control. .... 56

Figure 5-3, the charge distribution at  $0 \text{ V}$  and  $5 \text{ V}$  are shown to the left and right respectively. .... 56

Figure 5-4, to the left is the charge distribution at  $-5\text{V}$ , showing the accumulation. To the right is the band diagram at the same voltage level..... 57

Figure 5-5, the AC capacitance of the modulator..... 58

Figure 5-6, the modulator design with the superlattice. .... 59

Figure 5-7, the charge distribution in the modulator. To the left is at no voltage. To the right is at  $-5 \text{ V}$ . ..... 59

Figure 5-8, The charge accumulation in any of the InAs layers in the superlattice vs the voltage. .... 60

Figure 5-9, FDTD transmission of the modulator with and without a superlattice. .... 60

Figure 5-10, the GaAs/AlGaAs optical waveguide. .... 61

Figure 5-11, dispersion curve of the hybrid plasmonic waveguide (from previous chapter), also the symmetric and antisymmetric modes are shown..... 62

Figure 5-12, (a & c) shows the effective media permittivity real and imaginary parts respectively at different doping levels, and (b & d) shows the plain doped InAs permittivity real and imaginary parts respectively at different doping levels..... 63

*Figure 5-13, dispersion curves of the hybrid plasmonic modes, at four different doping levels, real (upper plot) and imaginary (Lower plot) parts. Also, dispersion curves of the optical modes are presented. .... 64*

Figure 5-14, wide band transmission of the modulator. The modulator response is divided into two parts, the first part is called the resonance regime, the second part is called the normal regime..... 66

Figure 5-15, Modal shape at resonance, at wavelength equal to 4.85  $\mu\text{m}$  in the Off state (to the left), and On State (to the right)..... 66

*Figure 5-16, The upper figure shows the modulator off state, while the lower figure shows the modulator on state. .... 67*

Figure 5-17, transmission at wavelength equal to 4.85 at 2.5V. .... 68

Figure 5-18, transmission at wavelength equal to 6.6 at 7.5V. .... 68

**List of Tables**

Table 3-1 refractive index of polymer and effective index of the plasmonic WG arms under 10V. ... 32

Table 3-2 Comparison between plasmonic modulators..... 34

**List of publications**

- A. A. R. Mohamed, L. A. Shahada and M. A. Swillam, "Electro-Optic Plasmonic Modulator with Direct Coupling to Silicon Waveguides," in IEEE Photonics Journal, vol. 9, no. 6, pp. 1-7, Dec. 2017.
- Ahmad B. Ayoub, Abd El-Rahman Nader, Mai Saad, Qiaoqiang Gan, Mohamed Swillam, "Fiber-optic-based interferometric sensor," Proc. SPIE 10110, Photonic Instrumentation Engineering IV, (20 February 2017).
- Abdalrahman Mohamed, Mohamed Swillam "Plasmonic Mach-Zehnder Modulator with Direct Coupling to Silicon Waveguides", 2015, Meta conference.
- Abdalrahman Mohamed, Mohamed Swillam "III-IV hybrid plasmonic electro-absorption modulator", a draft paper in the review process inside the group.

# Chapter 1: INTRODUCTION

## 1.1 OPTICAL MODULATORS

From the earliest work on optical circuits going back to the 1970s, images of an optical super-chip featuring a range of interconnected optical components for light generation, modulation, processing, detection and amplification have been envisioned Figure 1-1. Applications ranging from communication, sensing and computation are all waiting for a boost from such chips. One of the main components of these photonic chips is the optical modulators, which is the focus of this thesis.

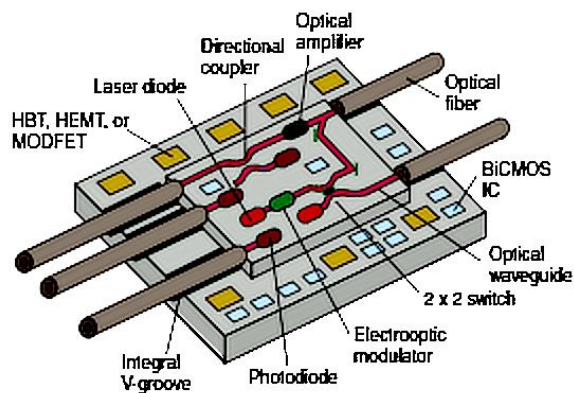


Figure 1-1 silicon based photonic circuit [1].

Optical modulators are devices which allow the manipulation of light propagating through by electrical signals, in other words, it transforms electrical signals to optical signals. Later on, light may be propagated through an optical waveguide, or carried in free space. Modulators are classified as amplitude modulators, phase modulators or polarization modulators, based on the feature of light that is being manipulated. Amplitude modulation is mainly discussed in this thesis.

There are two main types for amplitude modulation, the direct modulation and the exterior modulation. Direct modulation is done by modulating the current biasing the light source (e.g. a laser diode) directly. That is why light modulators are considered external light modulators, like what is usually done in fiber optic communications. Laser diodes are favorably required to have narrow linewidth; consequently, direct modulation is always not considered because of the high bandwidth

required for switching the current of the laser. As a result, optical modulators are always used after a light source to manipulate light.

## 1.2 MODULATORS CLASSIFICATION

Modulators are classified into two classes, depending on the characteristics of the material used to modulate the light beam: absorptive modulators and refractive modulators. The absorption coefficient (the imaginary part of the refractive index) of the material is modified in absorptive modulators, and the refractive index of the material is modified in refractive modulators.

The material's absorption coefficient in the modulator may be influenced by the Franz-Keldysh effect, the Quantum-confined Stark effect, excitonic absorption, Fermi level shifts, or adjustments in free carrier concentration. Generally, the modulator is called an electro-absorptive modulator if many such effects occur together.

The refractive index of a material is most commonly influenced by electro-optic effect. Other types of refractive modulators could have an acousto-optic or magneto-optic effect, or use the variations in the polarization of liquid crystals. The corresponding effect is named for the refractive modulators: i.e. electro-optic modulators, acousto-optic modulators etc. The role of either of the above types of refractive modulator is to manipulate the phase of light. A directional coupler or an interferometer may be used to transform the phase shift into amplitude modulation.

## 1.3 PLASMON POLARITONS

Surface plasmon polaritons (SPPs) (shown in Figure 1-2) are electromagnetic fields that is coupled to charge oscillations at metal dielectric interfaces, these fields can confine light in nanoscale regions that are considerably smaller than the wavelengths of light in the material [3]. The electromagnetic field perpendicular to the metal-dielectric interface decays steadily at a distance from the metal surface while preserving the long-range distribution of electromagnetic radiation across the surface. This interesting feature of SPPs enables subwavelength scale manufacturing of photonic components.

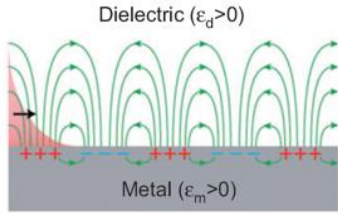


Figure 1-2, Surface plasmon polaritons

Surface plasmons (SPs) are classified into a localized type called localized surface plasmons (LSPs) and a propagating type called the propagating surface plasmon polaritons (PSPPs). For this work, only PSPPs would be listed for the purposes of optical signal communication and photonic circuits, so they are hereafter referred to as SPPs.

Thanks to the peculiar properties of SPPs, different forms of metallic nanostructures such as thin metal films [8], grooves [10], metal nanoparticle chains [4], hard metal wedges [14], metal slits [9] and chemically synthesized metal nanowires (NWs) [11], metal/insulator/metal (MIM) slabs, hybrid Bragg waveguide, metal strips, wire/spacer/film MIM structures, and hybrid plasmonic structures [15], were all introduced in nanophotonic applications.

## 1.4 ON CHIP MODULATORS

Two optical modulators are designed and discussed in this thesis for two different applications, the Lap On-Chip application and the optical interconnects application.

Silicon electronic circuits are reaching the fundamental physical limits in terms of both speed and data transmission rate [1], also heat dissipation is becoming a serious issue. The International Technology Roadmap for Semiconductors (ITRS) has highlighted interconnect scaling as a problem for the semiconductor industry. Some of the possible approaches to increase the data rate and lower heat dissipation in chips is the use of light, rather than electrons in data transmission [2]. Nonetheless, the viability of producing nanoscale photonics is restricted, because the diffraction limit of light is dominant when the size of a photonic system approaches the wavelength of light in the material, this is considered as the main challenge toward merging photonics and electronics.

The utilization of optical systems in electronic chips could solve the data rate issues, and loosens the heat dissipation problem. Such optical systems are called optical interconnects, which typically consists of a laser source, a modulator to transfer electrical signals to optical signals, optical waveguides to transmit data and detectors to retransform data to the electrical form [optical interconnects ref]. These systems are targeted to be built on the electronic chips for the communication between different electronic circuits, hereafter comes the term On-Chip optical systems and On-Chip optical modulators.

The optical interconnects and the lab On-Chip applications require different implementation technologies. Optical interconnects requires working at 1.55  $\mu\text{m}$  wavelength, and is required to be built with a technology that is compatible with the CMOS technology, hence silicon photonics is always the choice. On the other hand, lab On-Chip application requires working in the midinfrared region, as the absorption peaks of many of the molecules of interest for diagnostics is found in this wavelength range. The favorable technology for midinfrared region is the III-V semiconductor technology, as laser sources are efficiently built in this using III-V media.

Although photonics can allow for a huge performance gains for such applications, reducing the size of bulky photonic components is the major issue towards the implementation of photonic integrated circuits on electronic chips. Plasmon polaritons which tightly confine light at the metal-dielectric interface, can be a potential solution to this problem. Plasmonic On-Chip optical modulators are the focus of this thesis.

## 1.5 OBJECTIVES AND SCOPE OF THESIS

In this thesis, the plasmonic features are exploited to build optical modulators for two on-chip applications, first is interconnect applications, second is sensor photonic circuits. The first work is based on silicon on insulator platform to be compatible with the CMOS industry. The second is built for midinfrared wavelength region, as many sensor applications are built in this region, and it is based on III-V semiconductor media, to utilize the fact that the most efficient lasers in this domain is built on this technology, hence, opening the door for complete systems built on the same technology. The second piece of work was built by us starting from a new material configuration of the hybrid

plasmonic waveguide structure, so, a chapter is written to discuss the properties of this waveguide, before proceeding to the modulator.

In this thesis, the physics and design of plasmonic on chip optical modulators will be discussed. An electro-refractive and electro-absorption examples are designed, and computationally Modelled.

The rest of the thesis is organized as follows:

Chapter 2: Background and literature review

Chapter 3: Electro-Optic Plasmonic Modulator with Direct Coupling to Silicon Waveguides

Chapter 4: Negative & Positive Dispersion Engineering in Med Infrared Region for Hybrid Plasmonic Waveguide

Chapter 5: Mid-infrared Iii-V Electro-Absorption Hybrid Plasmonic Modulator

Chapter 6: conclusion



## 1.6 REFERENCES

- [1] Gramotnev DK, Bozhevolnyi SI . Plasmonics beyond the diffraction limit . *Nat Photonics* 2010 ; **4** : 83 – 91.
- [2] Zia R, Schuller JA, Chandran A, Brongersma ML . Plasmonics: the next chip-scale technology . *Mater Today* 2006 ; **9** : 20 – 27.
- [3] Barnes WL, Dereux A, Ebbesen TW . Surface plasmon subwavelength optics . *Nature* 2003 ; **424** : 824 – 830.
- [4] Maier SA, Kik PG, Atwater HA, Meltzer S, Harel E *et al* . Local detection of electromagnetic energy transport below the diffraction limit in metal nanoparticle plasmon waveguides . *Nat Mater* 2003 ; **2** : 229 – 232.
- [5] Quinten M, Leitner A, Krenn JR, Aussenegg FR . Electromagnetic energy transport via linear chains of silver nanoparticles . *Opt Lett* 1998 ; **23** : 1331 – 1333.
- [6] Alu A, Engheta N . Effect of small random disorders and imperfections on the performance of arrays of plasmonic nanoparticles . *New J Phys* 2010 ; **12** : 013015.
- [7] Liu N, Mukherjee S, Bao K, Li Y, Brown LV *et al* . Manipulating magnetic plasmon propagation in metallic nanocluster networks . *ACS Nano* 2012 ; **6** : 5482 – 5488.
- [8] Economou EN . Surface plasmons in thin films . *Phys Rev* 1969 ; **182** : 539 – 554.
- [9] Lopez-Tejiera F, Rodrigo SG, Martin-Moreno L, Garcia-Vidal FJ, Devaux E *et al* . Efficient unidirectional nanoslit couplers for surface plasmons . *Nat Phys* 2007 ; **3** : 324 – 328.
- [10] Bozhevolnyi SI, Volkov VS, Devaux E, Ebbesen TW . Channel plasmon-polariton guiding by subwavelength metal grooves . *Phys Rev Lett* 2005 ; **95** : 046802.
- [11] Sanders AW, Routenberg DA, Wiley BJ, Xia YN, Dufresne ER *et al* . Observation of plasmon propagation, redirection, and fan-out in silver nanowires . *Nano Lett* 2006 ; **6** : 1822 – 1826.
- [12] Ditlbacher H, Hohenau A, Wagner D, Kreibig U, Rogers M *et al* . Silver nanowires as surface plasmon resonators . *Phys Rev Lett* 2005 ; **95** : 257403.
- [13] Fang YR, Wei H, Hao F, Nordlander P, Xu HX . Remote-excitation surface-enhanced Raman scattering using propagating Ag nanowire plasmons . *Nano Lett* 2009 ; **9** : 2049 – 2053.
- [14] Boardman AD, Aers GC, Teshima R . Retarded edge modes of a parabolic wedge . *Phys Rev B* 1981 ; **24** : 5703 – 5712.

[15]Han ZH, Bozhevolnyi SI . Radiation guiding with surface plasmon polaritons . Rep Prog Phys  
2013 ; 76 : 016402.

## Chapter 2: BACKGROUND AND LITERATURE REVIEW

Optical modulators have a long history starting from being used in fiber communications. Early experiments used lithium niobate (LiNbO<sub>3</sub>) [1][2] exclusively because it possesses a strong electro-optic coefficient. III-V semiconductors such as devices based on gallium arsenide (GaAs) and indium phosphide (InP) was the usual platform. Lasers were mainly fabricated based on III-V media, which makes them interesting for the optical modulation.

Silicon (Si) dominance in the microelectronics industry, gradually led to Si photonic circuits being investigated, due to the possible integration with electronics. This work began late, in the mid-1980s for two reasons. First, Si is fundamentally limited as an optical element, as it is an indirect band gap, so non-traditional techniques for light generation must be examined. This research is making fast progress, silicon light-emitting diodes (LEDs) are now a fact [5], many researchers expect the Si laser's arrival. Secondly, Si's crystal structure does not show an electro-optic Pockels effect, which is the conventional way of implementing optical modulator.

Optical modulation in photonic circuits is applied through devices that trigger variations in optical intensity via absorption, or trigger shifts in the material's refractive index and hence the propagating wave phase, which can be transformed to a shift in intensity by an interferometer or resonant device.

The ideal way of introducing modulation is by adding an induced electric field change in the refractive index, since this indicates little to no current (and thus low power) and faster response. A change in the real part of refractive index, is named electrorefraction, and in the refractive index's imaginary part, is named electroabsorption. Pockels effect, Kerr effect, and Franz-Keldysh effect are the main electric field effects that are important in semiconductor materials.

### 2.1 SILICON OPTICAL MODULATORS

Silicon modulators are a corner block in the Silicon photonics industry since the beginning since initial research on simple waveguide technology [6][7][8][9]. A collection of interesting and/or important of the modulators tested since the mid-1980s will be discussed. Modulation depth, bandwidth, energy

consumption and footprint are the essential parameters for an optical modulator and, where applicable, these parameters are included in the discussion.

The early prototypes were based on Si guiding layers built from doped Si substrates, the latter with a decreased refractive index due to the influence of plasma dispersion. Waveguiding systems based on SOI platform became more common. The first plasma dispersion modulator in Si was suggested by [10]. The modulator is shown in Figure 2-1, is based on a Si rib waveguide, 1 mm long. The insertion loss of the modulator is less than 1 dB at 1.3  $\mu\text{m}$  wavelength. The structure is very similar to the nowadays silicon photonic modulators except for the buried n+ under the silicon dioxide layer that allows for vertical current streaming.

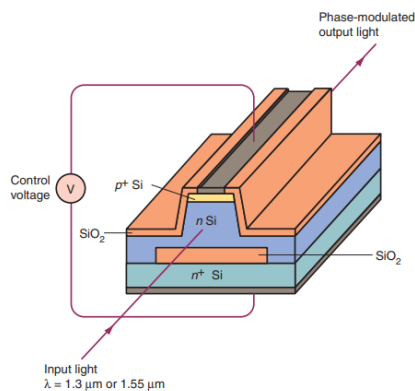


Figure 2-1 Proposed SOI p+-n-n+ channel-waveguide electro-optical phase modulator [10].

In 1993, utilizing a single mode SiGe rib waveguide [11] an MZI were developed with a PIN device. The modulation depth at a wavelength of 1.3  $\mu\text{m}$  was found to be -10 dB, with a current of 150 mA, the lowest value recorded at the time. But their device's response time wasn't recorded. Silicon photonic based modulators were mostly used in optical modulators in the mid of nineties.

In 1997, a Si modulator is introduced based on three-terminals on a low-loss single-mode SOI waveguide but with the buried oxide layer eliminated in the modulator 's active area Figure 2-2 [12].

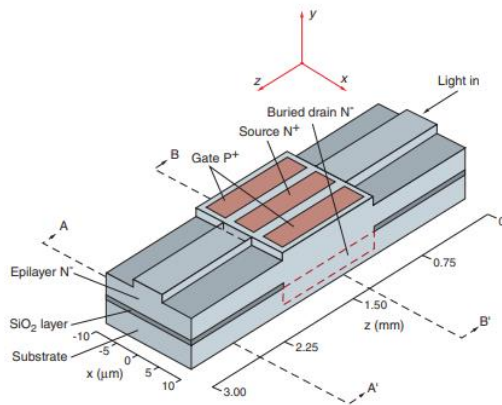


Figure 2-2 Three-terminal modulator proposed by [12].

The device was technically evaluated and the three-terminal electronic configuration is, according to the scientists, considerably more effective than two-terminal PIN diode-based modulators, a close inference to the previously drawn by [13][14][15]. A 20 percent amplitude modulation at an injection power of around 126 mW and a switching time of 5.6 ns was recorded.

In fact, it demonstrated a rather high figure of merit when the system was utilized as a phase modulator. With a driving power of 43 mW and a switching period of less than 3.5 ns (> 100 MHz) the expected output was around 215 °/Vmm. This was a very optimistic prediction at the time for a modulator centered on a broad rib waveguide. For the rib diameter, Si layer thickness and etch depth, the proposed modulator has dimensions of 6 μm, 6 μm, and 1.5 μm, respectively.

In 2000, a basic two-terminal PIN modulator based on a 5.5 μm SOI rib waveguide was revived using computer simulation. It is expected that substantial optimization is feasible for a two-terminal system. A raise in p<sup>+</sup> and n<sup>+</sup> doping concentrations from 1E19cm<sup>-3</sup> to 1E20cm<sup>-3</sup> will result in a decrease in drive current from 63 mA to 8 mA.

Scientists at Intel [16] have experimentally demonstrated a Si-based optical modulator with a bandwidth that for the first time approaches 1 GHz. It is a major achievement in Si photonics and has received considerable public coverage [17]. This system strongly resembling a CMOS transistor.

## 2.2 PLASMONIC MODULATORS

The scaling of present modulator designs discussed in previous section to micrometer and nanometer scale is not possible due to poor electro-optic effects. Plasmonics can offer new modulator designs that are substantially more compact and thus effective in power.

Active plasmonics was first used in proposing SPP modulation by a light-induced phase change in a nanoscale layer of a metal / Gallium SPP waveguide [21]. SPP fields are tightly confined to metal surfaces, and thus extremely susceptible to shifts in refractive index [22]. The basic active plasmonic concept is a temporary change in the refractive index of either the metal or dielectric part of an SPP waveguide, caused by external control excitation modulate the intensity and/or phase of a propagating SPP [24].

A modulator based on SPP was recorded in CdSe quantum dots in 2007 [18]. Quantum dots covering the surface of a silver waveguide in their ground state have no effect on the transmission of an SPP signal at a wavelength of  $1.426\mu\text{m}$ . However, when stimulated at  $514.5\text{ nm}$  by a co-propagating pump SPP they are absorbent at the wavelength of the probe and attenuate the SPP electrode. A 12 percent increase (0.55 dB) was reported in a device's optical signal efficiency with a  $3.6\ \mu\text{m}$  SPP waveguide duration with an optical pump strength of  $600\text{W/cm}$ ; It was achieved at modulation frequencies of up to 25 MHz (the height of the detector apparatus), suggesting a fixed cycle period of 40 ns.

The next year, a non-volatile plasmonic transition utilizing photochromic molecules as the active part was shown [19] the molecules were located inside the polymer part of an aluminum / PMMA waveguide for an SPP signal at  $633\text{ nm}$ ; they were transferred between stable absorbing and transparent states utilizing  $6\text{ mW / cm}$  free-space optical pump beams.

An electro-plasmonic modulator was reported [20], the application of a bias (up to 45 V) across a silver/barium-titanite SPP waveguide induces domain switching in the ferroelectric BaTiO thin film and modifies its refractive index. As part of an interferometric device structure with a length of between  $0.5\text{ and }5.3\ \mu\text{m}$  such switching modulates the optical output at  $688\text{ nm}$  by up to 15% (0.7 dB).

The modulation of a femto-second SPP signal via the direct optical excitation of metal was demonstrated [25]. Wavelength probe experiments at 780 nm (and a subsequent study covering the range from 765 to 810 nm [26]) reveal a nonlinear interaction between probe SPP and pump light that takes place in the skin layer of the metal; It produces up to 35% ( 1.3 dB) modulation of the probe for a pump fluence of 13 mJ.cm over an SPP propagation distance of 5 $\mu$ m.

A metal-oxide-semiconductor (MOS) field-effect plasmonic modulator operating at 1.55  $\mu$ m was reported [27]. The device employs a four-layer metal-MOS-metal waveguide structure that supports both photonic and plasmonic modes, and has a transmission coefficient determined by interference between the two. Switching times are found to be shorter than the 10 ns limit of the experimental apparatus. A peak modulation depth of 4.56 dB is observed at 0.75 V in a device 2.6 $\mu$ m long. the fundamental limit on switching speed is the charge accumulation. The plasmonic modulator could operate at gigahertz frequencies.

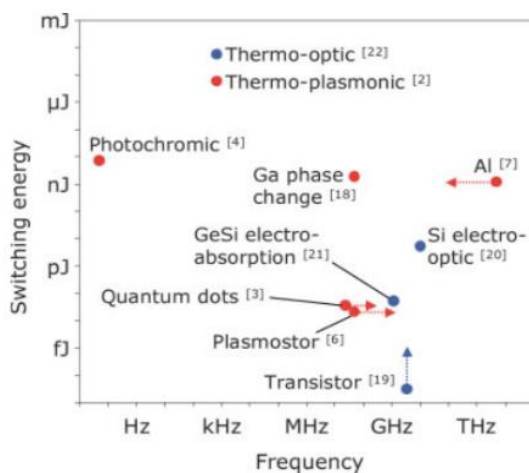


Figure 2-3 The figure shows the switching energy vs operating frequency of different types of optical modulators.

### 2.3 MIDINFRARED MODULATORS

There is no much research work done on modulators for the midinfrared region. Few groups tried to extend the Si or Ge based modulators to the midinfrared region [28][29]. Expanding the telecommunication wavelength range to higher than 2  $\mu$ m is one motivation for such research [30]. Also, longer wavelengths can be utilized in free-space communications modulator, signal processing and switching applications [31]. In addition to the need for such modulators for sensor photonic

circuits [32] at the whole midinfrared region from 2 to 20  $\mu\text{m}$ . SOI carrier injection modulators with speed up to 3 Gb/s at 2165 nm wavelength [34], and GOI modulators at 1950 nm wavelength [33] have been demonstrated.

In the near-IR, high-speed modulators typically employ free-carrier depletion in a PN junction [35], and use either a Mach-Zehnder interferometer (MZI) or ring resonator to convert the phase change into an intensity change. An MZI-based PN junction modulator in the SOI platform has been demonstrated at 1950 nm. The device operates at carrier depletion mode, a modulation efficiency of 2.02 V.cm at 1550 nm and 2.68 V.cm were measured. An open eye diagram at 20 Gb/s with a 5.8 dB extinction ratio were measured [31].

The free carrier effect for Si and Ge were Semi-empirically presented in [36] and [37] respectively. These equations predict that the free carrier effect is approximately proportional to the square of the wavelength in both materials, with Ge generally stronger than Si. Modulators in SOI and GOS technologies were built and characterized at 3.8  $\mu\text{m}$  wavelength [31]. The modulators were based on PIN diodes integrated with a waveguide, where carrier injected from the diode into the waveguide changes the imaginary part of the waveguide core, which means changes its absorption. The SOI modulator was 2 mm long, and the GOS modulator was 1 mm long. They both achieve a modulation depth higher than 30 dB, the SOI modulator achieves an insertion loss of 2.8 dB [31].

As it is clear from this short summary of Si and Ge based midinfrared modulators, there are few work done in this domain, and structures are still having a very big footprint, and high insertion, losses which is not suitable for working in Lap-On-Chip applications.

## REFERENCES

- [1] Kondo J et al 2005 High-speed and low-driving-voltage thin-sheet X-cut LiNbO<sub>3</sub> modulator with laminated low-dielectric-constant adhesive IEEE Photon. Technol. Lett. 17 2077–9.
- [2] Reed, G. T., and Weiss, B. L., Electron. Lett. (1987) 23, 424.
- [3] Pavesi, L., et al., Towards the First Silicon Laser, NATO Science Series, Kluwer.
- [4] Academic Publications, Dordrecht, (2003).



- [5] Poleman, A., et al., J. Appl. Phys. (1995) 77 (3), 1256.
- [6] D. J. Albares, R. A. Soref, "Silicon-On-Sapphire Waveguides," Proc. SPIE 0704, Integrated Optical Circuit Engineering IV, (10 March 1987); <https://doi.org/10.1117/12.937191>
- [7] R. A. Soref, J. Schmidtchen and K. Petermann, "Large single-mode rib waveguides in GeSi-Si and Si-on-SiO<sub>2</sub>," in IEEE Journal of Quantum Electronics, vol. 27, no. 8, pp. 1971-1974, Aug. 1991, doi: 10.1109/3.83406.
- [8] B. L. Weiss, G. T. Reed, S. K. Toh, R. A. Soref and F. Namavar, "Optical waveguides in SIMOX structures," in IEEE Photonics Technology Letters, vol. 3, no. 1, pp. 19-21, Jan. 1991, doi: 10.1109/68.68035.
- [9] G.T. Reed, Li Jinhua, C.K. Tang, Lin Chenglu, P.L.F. Hemment, A.G. Rickman, Silicon on insulator optical waveguides formed by direct wafer bonding, Materials Science and Engineering: B, Volume 15, Issue 2, 1992, Pages 156-159, ISSN 0921-5107, [https://doi.org/10.1016/0921-5107\(92\)90048-E](https://doi.org/10.1016/0921-5107(92)90048-E).
- [10] Richard A. Soref and Brian R. Bennett "Kramers-Kronig Analysis Of Electro-Optical Switching In Silicon", Proc. SPIE 0704, Integrated Optical Circuit Engineering IV, (10 March 1987); <https://doi.org/10.1117/12.937193>.
- [11] U. Fischer, B. Schuppert and K. Petermann, "Integrated optical switches in silicon based on SiGe-waveguides," in IEEE Photonics Technology Letters, vol. 5, no. 7, pp. 785-787, July 1993, doi: 10.1109/68.229806.
- [12] A. Cutolo, M. Iodice, P. Spirito and L. Zeni, "Silicon electro-optic modulator based on a three terminal device integrated in a low-loss single-mode SOI waveguide," in Journal of Lightwave Technology, vol. 15, no. 3, pp. 505-518, March 1997, doi: 10.1109/50.557567.
- [13] C. K. Tang, G. T. Reed, A. J. Walton and A. G. Rickman, "Low-loss, single-mode optical phase modulator in SIMOX material," in Journal of Lightwave Technology, vol. 12, no. 8, pp. 1394-1400, Aug. 1994, doi: 10.1109/50.317527.
- [14] Tang, C. K., et al., Mat. Res. Soc. Symp. Proc. (1993) 298, 247.
- [15] Tang, C. K., and Reed, G. T., "Highly efficient optical phase modulator in SOI waveguides" Electron. Lett. (1995) 31 (6), 451.
- [16] Liu, A., Jones, R., Liao, L. et al. A high-speed silicon optical modulator based on a metal–oxide–semiconductor capacitor. Nature 427, 615–618 (2004). <https://doi.org/10.1038/nature02310>
- [17] Soref, R. A., and Bennett, B. R., Proc. SPIE (1986) 704, 32.

- [18] Barnes WL, Dereux A, Ebbesen TW . Surface plasmon subwavelength optics . *Nature* 2003 ; **424** : 824 – 830.
- [19] Maier SA, Kik PG, Atwater HA, Meltzer S, Harel E *et al* . Local detection of electromagnetic energy transport below the diffraction limit in metal nanoparticle plasmon waveguides . *Nat Mater* 2003 ; **2** : 229 – 232.
- [20] Quinten M, Leitner A, Krenn JR, Aussenegg FR . Electromagnetic energy transport via linear chains of silver nanoparticles . *Opt Lett* 1998 ; **23** : 1331 – 1333.
- [21] Gramotnev DK, Bozhevolnyi SI . Plasmonics beyond the diffraction limit . *Nat Photonics* 2010 ; **4** : 83 – 91.
- [22] Chen JJ, Sun CW, Hu XY . Nanoscale all-optical devices based on surface plasmon polaritons . *Chinese Sci Bull* 2014 ; **59** : 2661 – 2665.
- [23] Han ZH, Bozhevolnyi SI . Radiation guiding with surface plasmon polaritons . *Rep Prog Phys* 2013 ; **76** : 016402.
- [24] Zia R, Schuller JA, Chandran A, Brongersma ML . Plasmonics: the next chip-scale technology . *Mater Today* 2006 ; **9** : 20 – 27.
- [25] Liu N, Mukherjee S, Bao K, Li Y, Brown LV *et al* . Manipulating magnetic plasmon propagation in metallic nanocluster networks . *ACS Nano* 2012 ; **6** : 5482 – 5488.
- [26] Chang DE, Sorensen AS, Hemmer PR, Lukin MD . Strong coupling of single emitters to surface plasmons . *Phys Rev B* 2007 ; **76** : 035420.
- [27] Alu A, Engheta N . Effect of small random disorders and imperfections on the performance of arrays of plasmonic nanoparticles . *New J Phys* 2010 ; **12** : 013015.
- [28] M. Nedeljkovic, S. Stanković, C. Mitchell, A. Z. Khokhar, S. Reynolds, D. J. Thomson, F. Y. Gardes, C. Littlejohns, G. T. Reed, and G. Z. Mashanovich, "Mid-infrared thermo-optic modulators in SOI," *IEEE Photonics Technol. Lett.* 26(13), 1352–1355 (2014).
- [29] J. Chiles and S. Fathpour, "Mid-infrared integrated waveguide modulators based on silicon-on-lithium-niobate photonics," *Optica* 1(5), 350–355 (2014).
- [30] R. Soref, "Enabling 2  $\mu\text{m}$  communications," *Nat. Photonics* 9(6), 358–359 (2015).
- [31] G. Z. Mashanovich, M. Nedeljkovic, J. Soler-Penades, Z. Qu, W. Cao, A. Osman, Y. Wu, C. J. Stirling, Y. Qi, Y.X. Cheng, L. Reid, C. G. Littlejohns, J. Kang, Z. Zhao, M. Takenaka, T. Li, Z. Zhou, F. Y. Gardes, D. J. Thomson, and G. T. Reed, "Group IV mid-infrared photonics [Invited]," *Opt. Mater.*

- [32] M. Nedeljkovic *et al.*, "Mid-Infrared Thermo-Optic Modulators in Sol," in *IEEE Photonics Technology Letters*, vol. 26, no. 13, pp. 1352-1355, July 1, 2014, doi: 10.1109/LPT.2014.2323702.
- [33] J. Kang, M. Takenaka, and S. Takagi, "Novel Ge waveguide platform on Ge-on-insulator wafer for mid-infrared photonic integrated circuits," *Opt. Express* 24(11), 11855–11864 (2016).
- [34] M. A. Van Camp, S. Assefa, D. M. Gill, T. Barwicz, S. M. Shank, P. M. Rice, T. Topuria, and W. M. J. Green, "Demonstration of electrooptic modulation at 2165nm using a silicon Mach-Zehnder interferometer," *Opt. Express* 20(27), 28009–28016 (2012).
- [35] D. J. Thomson, L. Shen, J. J. Ackert, E. Huante-Ceron, A. P. Knights, M. Nedeljkovic, A. C. Peacock, and G. Z. Mashanovich, "Optical detection and modulation at 2 $\mu$ m-2.5 $\mu$ m in silicon," *Opt. Express* 22(9), 10825–10830 (2014).
- [36] M. Nedeljkovic, R. Soref, and G. Z. Mashanovich, "Free-carrier electrorefraction and electroabsorption modulation predictions for silicon over the 1-14- $\mu$ m infrared wavelength range," *IEEE Photonics J.* 3(6), 1171–1180 (2011).
- [37] M. Nedeljkovic, R. Soref, and G. Z. Mashanovich, "Predictions of free-carrier electroabsorption and electrorefraction in germanium," *IEEE Photonics J.* 7(3), 1–14 (2015). Vol 8, 2276-2286 (2018).
- [38] Vol. 8, No. 8 | 1 Aug 2018 | OPTICAL MATERIALS EXPRESS 2282.

# Chapter 3: ELECTRO-OPTIC PLASMONIC MODULATOR WITH DIRECT COUPLING TO SILICON WAVEGUIDES

**ABSTRACT:** A novel plasmonic Mach-Zehnder Interferometer is proposed with a nonlinear polymer. Orthogonal junction coupling between silicon and plasmonic waveguides is exploited to omit the need for tapers, and in turn, reduce the footprint. An extinction ratio of about 16 dB is produced at a voltage-length product of 47 V $\mu$ m. An insertion loss of 3.38 dB is achieved including the coupling to and from the silicon access waveguide. The orthogonal coupling provides wideband operation, high efficiency, low loss and compact size for our design.

**Index Terms:** Integrated Optics Devices, Modulators, Electro-Optical Devices, Surface Plasmons.

## INTRODUCTION

Electrical interconnects limit the processors computational power, due to the RC delay in communication within the cores of the processor and between different cores. Optical Interconnects that have the privilege of working at much higher speeds offers a good solution for such problem [1,2]. A key component in any on chip optical system is the electro-optic modulator. High compactness, low Power consumption, large extinction ratio, and high speed are the most desirable properties of the electro-optic modulator.

Silicon photonics technology has attracted considerable attention in the last decade due to its ability to fabricate low loss waveguide based components. Modulation, in general, occurs through utilizing nonlinear effect, or through utilizing index change induced due to free carrier injection [3-6]. However, silicon photonic devices miniaturizing in the nano-scale is not easy due to the diffraction limit.

Plasmonics, on the other hand, has the unique ability of confining light in metal-dielectric interfaces in the nano scale. Hence, it can increase the light-mater interaction and allow for shorter devices compared to silicon photonics [7]. On the other hand, plasmonics suffer from high propagation losses and should be compact in size to alleviate this drawback. A hybrid technology that exploits the low path losses advantage of silicon photonics and the tight light confinement of plasmonic devices can be an attractive platform specially for on chip modulators [6,8], such a hybrid platform is known as the hybrid plasmonic

platform. Plasmonic crystal nano-cavities [9\*], hybrid photonic-plasmonic resonator [10\*], optical trapping device [11\*] and a biosensing application [12\*] have been demonstrated as applications from the hybrid photonic plasmonic systems.

Plasmonic modulators, can be built using various configurations including resonance topology, electro-absorption, and interference mechanism. Plasmonic resonators have a relatively small footprint, and low power consumption [13]. However, they suffer from high sensitivity to temperature and process variations, requiring them stabilization circuitry, and in turns more power and area consumption [14]. On the other hand, Mach-Zehnder doesn't suffer from temperature and process variations, as these variations usually cancel out in the symmetric arms of the Mach-Zehnder [15]. Electro-absorption modulator, on the other hand, dissipates more heat than the other modulators [16,17]. Graphene and Indium Tin oxide (ITO) are widely used for such applications [18-22]. Lastly, interferometer modulators including Mach-Zehnder modulators (MZM) for example, are low power consumers, but they lack the small footprint advantage of their competitors and hence higher insertion losses are expected [22-24].

In this thesis, we utilize the advantages of both the plasmonic organic MZM and the orthogonal junction coupler presented in [25,26]. These two platforms together are able to make a good compromise between modulator length, footprint, extinction ratio, insertion loss, and energy consumption relative to the previous works, as will be shown latter. The orthogonal junction enables direct coupling between silicon interconnects used in routing data, and plasmonic waveguides of the MZM, without the need for a tapering or any special junction, this advantage is the main source of enhancement in our design.

In the next section, we present the working principle of the modulator. The third section presents the design methodology and optimization process of the modulator. The fourth section presents the results accompanied by a discussion of the work significance.

### **3.1 OPERATION PRINCIPLE**

The MZM device consists of input silicon waveguide, coupled to a plasmonic slot orthogonal junction, that is connected to the plasmonic slot arms of the MZM. Lastly the MZM arms are coupled to the output silicon waveguide again through an orthogonal coupler, as shown in Figure 3-1. The waveguides are

optimized such that lateral momentum component of the silicon waveguide mode matches the momentum of the plasmonic slot waveguide (PSW) to ensure maximum coupling between the two waveguides. This approach has theoretically and experimentally been verified to provide efficient, wide band, non-resonant coupling from/to silicon waveguides to/from PSWs [25,26].

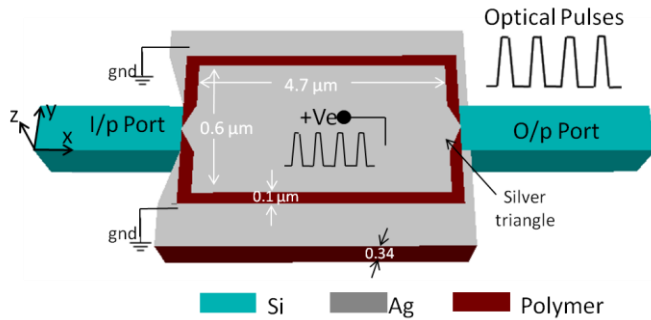


Figure 3-1 The MZM, with input and output silicon waveguides, the modulator arms are plasmonic slot waveguides filled with nonlinear polymer, with two silver triangles at the input and output. The  $x$ - $y$  plane contains the top plane of the modulator.

The plasmonic waveguide core is filled with a nonlinear electro-optic polymer (EOP) that exhibits the Pockels effect. If no voltage is applied, the light propagates to the combiner, where the fields interfere constructively, Figure 3-2(a). Once the voltage is applied, the refractive indices of the upper and lower paths differ, so the light propagate in each arm at different speed. The length of the plasmonic waveguide is designed to induce sufficient phase difference between the two paths to create a destructive interference at the combiner as shown in Figure 3-2(b).

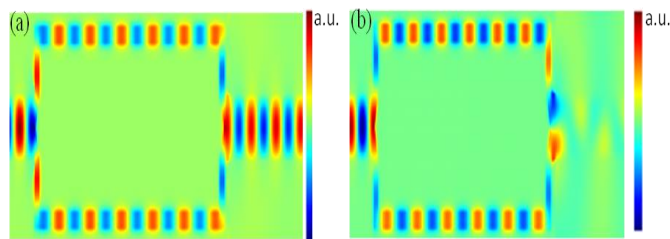


Figure 3-2 The  $z$ -component of the magnetic field ( $H_z$ ) at wavelength equals to  $1.55\mu\text{m}$  for the On state of the modulator (a), and the Off state (b).

Positive voltage is applied on the middle silver island, and a ground is applied on the exterior silver islands as shown in Figure 3-1. Accordingly, the electric field direction is outward from the middle metal island. The PSWs along the  $y$ -axis located at the splitter and the combiner, have an electric field direction in the

negative and positive x-direction respectively. This biasing method is called the push-pull configuration. Only the plasmonic waveguide parts along the x-axis in each arm will have a different field direction, in turns, they will be the only contributors in creating the phase difference accumulation.

It is worth noting that the Silicon-PSW orthogonal junction designed in [25,26] were optimized, where the slot was air filled. Now the slot is filled with the EOP which increases the momentum of the plasmonic mode inside the slot. This required a modification of the original design to allow for better matching, efficient splitting, and minimize the reflection to the main waveguide. Accordingly, the design has been optimized with two major modifications. The first one, is the addition of silver triangles to the middle metal island at the splitter and combiner. The silver triangles help in guiding the power in the splitter and out of the combiner. Also, they decrease the reflections from the orthogonal junction combiner which cause an undesired cavity effect for the proper work of the MZM. The base side of the isosceles silver triangle is equal to the width of the silicon waveguide. The second modification is using a 100 nm flat metal surface instead of the tapered one at the combiner, as shown in Figure 3-1, this is found more capable of distributing the power at the output of the silicon waveguide, such that the fields interfere destructively in a more efficient way, which enhances the extinction ratio.

### **3.2 OUR NOVEL DESIGNS**

A full electromagnetic analysis based on the finite-difference time-domain method is utilized to verify the design concept and optimize the design using [27]. The smallest mesh size is 10 nm. 2D simulations were used as a preliminary step for 3D simulations. Throughout 2D simulations, the Si on SiO<sub>2</sub> waveguide were modeled using the effective index method. In 3D simulations, the refractive index of Si and SiO<sub>2</sub> were chosen to be 3.45 and 1.45 respectively. The Johnson-Christy material model is used for silver [28], which is an experimentally verified model. The effect of the angle of the wedge with the silicon waveguide at the input side is minor as long as it is between 45 degrees and 80 degrees. The polymer used is Dispersive Red 1-poly-methyl-methacrylate (DRI-MMA) side chain copolymer [30]. The electro-optic side chain copolymers are known to be stable and can be used in long term photonic devices [30]. The thickness of the polymer layer is the same as surrounding silver.

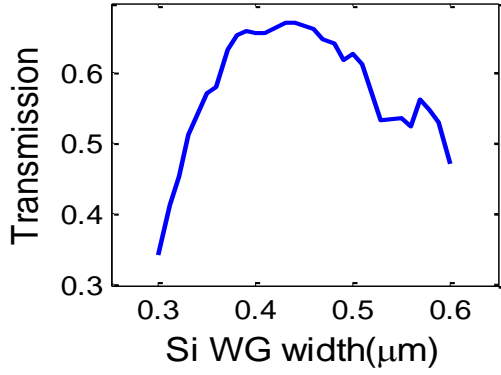


Figure 3-3 The transmission (output power/input power) of the modulator versus the width of the silicon waveguide (Si WG) at a height equal to 340 nm, and wavelength equal to 1.55 μm at zero voltage (On state).

Figure 3-3 shows the transmission of the modulator Vs Si waveguide width, at a slot gab size of 100 nm, with arbitrary arm lengths, the 400 nm is chosen for maximum coupling. The height of the silicon waveguide was chosen to be 340 nm to match a typical sold silicon on insulator (SOI) wafer. The refractive index change of the polymer by Pockels effect follows Eq.(1) [29].

$$n = n_0 \pm \frac{1}{2} \times r_{33} \times n_0^3 E$$

(1)

Where  $n_0$  is the refractive index of the polymer at no voltage, it is equal to 1.6,  $r_{33}$  is the electro-optic coefficient of first order nonlinearity of the polymer, it is equal to 300 pm/V [30], and  $E$  is the electric field across the polymer. The electric field is  $V/g$ , where  $V$  is the voltage difference across any of the two arms of the Mach-Zehnder,  $g$  is the slot width of the plasmonic waveguide. The sign in Eq.(1) can be positive or negative according to the direction of the applied electric field. We chose  $g$  to be 0.1 μm to be convenient for future fabrication. The device is feasible to be fabricated using electron beam lithography similar to the design in [24].

By applying 10V on the middle silver area, the refractive indices of the polymer of each arm are calculated using Eq.(1), and the effective indices of the plasmonic waveguides are calculated using modal analysis [27]. Both refractive and effective indices are shown in Table 3-1. The large variation in the effective index is an evidence on the high light-matter interaction and confinement.



Table 3-1 refractive index of polymer and effective index of the plasmonic WG arms under 10V.

	Arm(1)	Arm(2)	$\Delta n$
<b>Refractive index</b>	1.6614	1.5386	0.1228
<b>Effective index</b>	2.2464	2.0667	0.1797

The phase delay is related to the propagation constant through  $\Delta\beta.L = \phi$ , where L is the Mach-Zehnder arm length,  $\phi$  is the phase difference on the ends of each arm, and  $\beta$  is the propagation constant of the plasmonic mode. The length of the modulator is as given by Eq. (2).

$$L = \frac{\pi}{\Delta\beta} = \frac{\lambda}{2\Delta n_{eff}}$$

The length is calculated to be 4.33 $\mu\text{m}$ . Through 3D simulations, on applying 10V, the optimum value for the length of the arms, at which the modulator has minimum transmission, was found to be 4.7  $\mu\text{m}$ . Consequently the length of the plasmonic waveguide along the x direction is 4.7  $\mu\text{m}$  and the sides along the y direction were chosen to be 0.6  $\mu\text{m}$ , which is lower than previous published work as will be shown latter. The main performance enhancer is the addition of the orthogonal coupling junctions which is shorter than the taper junctions used before [24].

### 3.3 MODULATOR CHARACTERISTICS

To be able to quantify the performance of an optical modulator, few important measures should be calculated. The main parameters are the extinction ratio, insertion loss, dimensions, bandwidth, energy per bit, and the reflections. Each of these parameters are defined, compared and discussed with the state of the art values in the following subsections.

The main output of our analysis - from which we will discuss most of the modulator metrics - is the transmission (output power/input power) of the modulator, shown in Figure 3-4. The transmission curve was calculated from 3D simulations for two cases. The first at biasing voltage equal to 10V, and the second for biasing voltage equal to 6V. The main parameters of the modulator is extracted in Table 3-2 for the 1.55  $\mu\text{m}$  wavelength. The parameters for state of the art designs in literature are added to the same table. The designs presented in the table are: [23,25] which are plasmonic MZM with tapered couplers of different configurations, and [20] which is an electro-absorption modulator.

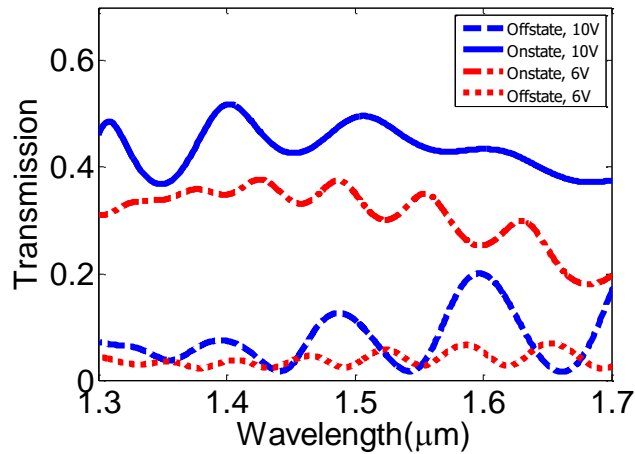


Figure 3-4 The transmission (output power/input power) in the On and Off states. The blue solid is for the 10V modulator whose length is 4.7  $\mu\text{m}$ . The red dashed is for the 6V modulator whose length is 8.1  $\mu\text{m}$ .

Extinction ratio is a key parameter in modulators, it quantifies the strength of modulation by measuring the difference between the output power in the on and off states. 3D simulations were done to get accurate values for extinction ratio at 10V and 6V biasing. An extinction ratio of 15.8 dB is calculated at 10V, and approximately 11 dB is calculated at 6V, both at 1.55 $\mu\text{m}$ .

To show the superiority of this performance, we compared our results to state of the art MZM. Our device has higher extinction ratio than the 6dB presented in [24] and the 7.3 dB presented in [23], as shown below in Table 3-2. Both designs presented in [23, 24] use different configurations of tapered couplers; that shows the effectiveness of using orthogonal coupling. Also we compared our work to a state of art electro-absorption modulator presented [20], and our device also shows higher extinction ratio as shown in Table 3-2 below.

Insertion loss is a critical measure for the optical losses in the device. Higher losses in any of the devices in an interconnect system, means more energy consumption in the whole processor; energy consumption is a critical issue in processors. The optical losses include the coupling and waveguide and material losses. Our device shows 3.38 dB and 4.6 dB at 10V and 6V biases, respectively. This performance is a step ahead the previously published work in plasmonic MZM as shown in Table 3-2 below.

*Table 3-2 Comparison between plasmonic modulators*

<b>Comparison Parameters</b>	<b>Our Work at 10V</b>	<b>Our Work at 6V</b>	<b>C.Haffner (2015)[24]</b>	<b>Shiyang Zhu (2010) [16]</b>	<b>Volker J. Sorger(2012)[20]</b>
<b>Extinction Ratio</b>	15.8 dB	11 dB	6 dB	7.3 dB	5 dB
<b>Insertion Loss</b>	3.38 dB	4.6 dB	5 dB	8 dB	1 dB
<b>Energy Consumption</b>	40.82 fJ bit <sup>-1</sup>	25.5 fJ bit <sup>-1</sup>	25 fJ bit <sup>-1</sup>	-	56 fJ bit <sup>-1</sup>
<b>Voltage</b>	10 V	6 V	6 V	5.6 V	4 V
<b>Length</b>	4.7 μm	8.1 μm	10 μm	3.7 μm	5 μm

A main target of our work is to enhance the size of the MZM. the main parameter that quantify the size of a MZM is the voltage length product. Our device shows 47 Vμm voltage length product, which is 21.5% lower than the state of the art plasmonic MZM presented in [24].

Optical bandwidth can be quantified from the transmission response in Figure 3-4, the 6V biased modulator, shows a wide band operation especially for the region starting from 1.3μm till 1.55μm. The 10V biased modulator shows a narrow band response, due to the ripples in the response. These ripples in the transmission response is due to a resonating wave that bounces between the two orthogonal

junctions. This resonance effect is more evident in the 10V modulator because it has a shorter length, in turns lower losses and higher quality factor. Electrical bandwidth determines the maximum bit rate of the modulator. Since our device is smaller than the one reported in [24] and the same electro-optic material is used, then it is estimated to have at least the same bit rate that exceeded 54 Gbit/s.

The energy per bit consumption for the modulators in optical interconnects should be as low as 50 fJ bit<sup>-1</sup> [31]. We estimated the energy consumption using a capacitance model, the capacitance is calculated analytically. Our modulator is below this limit at both the 10V and 6V biased modulators. In comparison to the modulators presented in table(3), our 6V biased modulator shows similar energy per bit value to [24], and both our devices show lower values than the electro-absorption modulator presented in [20]. Resonators show lower energy consumption, but as mentioned before, resonators are much less stable against process and temperature variations [14, 15].

Lastly, the coupling losses in both modulator arms ranges between 1.87 dB to 0.97 dB in the range of wavelength between 1.4 μm to 1.6 μm, in the on state of the 10V biased modulator. In the off state, the coupling decreases due to the effective index contrast between the silicon and plasmonic waveguides.

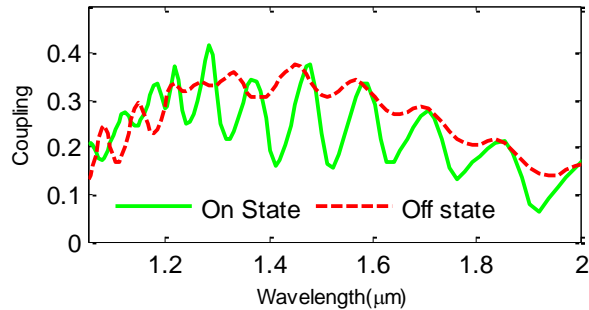


Figure 3-5 The two curves show the normalized coupling in any of the two arm, in the on (solid green) and off (dashed red) states. Both are for the 10V modulator (the legend is for both graphs).

### 3.4 CONCLUSION

An organic plasmonic Mach-Zehnder modulator was presented. We took advantage of the orthogonal junction coupling technique. The footprint of the modulator is decreased to  $0.6\mu\text{m} \times 4.7\mu\text{m}$  by the omission of the tapering sections used before [24] to couple in and out of plasmonic waveguides.

Extinction ratio of 15.8 dB and insertion loss of 3.38 dB at 10 volts was achieved in the 3D simulations. The voltage length product for the modulator is 47 V $\mu$ m. The orthogonal junction coupler enhances the extinction ratio and insertion loss of the organic Mach-Zehnder plasmonic modulator, while keeping the voltage length product approximately the same.

#### Acknowledgment

This work was made possible by a NPRP award [NPRP7-456- 1- 085] from the Qatar National Research Fund (member of the Qatar Foundation). The statements made herein are solely the responsibility of the authors.

#### REFERENCES

- [1] Semiconductor Industry Association, The International Technology Roadmap for Semiconductors, 2013. [Online].
- [2] Available: <http://www.itrs2.net/2013-itrs.html>
- [3] Semiconductor Industry Association, The International Technology Roadmap for Semiconductors, 2015. [Online].
- [4] Available: <http://www.itrs2.net/2013-itrs.html>
- [5] D. Korn *et al.*, "Silicon-organic hybrid (SOH) IQ modulator using the linear electro-optic effect for transmitting 16QAM at 112 Gbit/s," *Opt. Exp.*, vol. 21, pp. 13219–13227, 2013.
- [6] H. Xu *et al.*, "High-speed silicon modulator with band equalization," *Opt. Lett.*, vol. 39, pp. 4839–4842, 2014.  
A. Dhiman, "Silicon photonics: A review," *IOSR J. Appl. Phys.*, vol. 3, pp. 67–79, 2013.
- [7] G. T. Reed, G. Mashanovich, F. Y. Gardes, and D. J. Thomson, "Silicon optical modulators," *Nature Photon.*, vol. 4, pp. 518–526, 2010.
- [8] D. K. Gramotnev and S. I. Bozhevolnyi, "Plasmonics beyond the diffraction limit," *Nature Photon.*, vol. 4, pp. 83–91, 2010.
- [9] Z. Ma, Z. Li, K. Liu, C. Ye, and V. J. Sorger, "Indium-tin-oxide for high-performance electro-optic modulation," *Nanophotonics*, vol. 4, pp. 198–213, 2015.

- [10]X. Yang *et al.*, “Hybrid photonic Plasmonic crystal nanocavities,” *ACS Nano*, vol. 5, pp. 2831–2838, 2011.
- [11]Y.-F. Xiao *et al.*, “Strongly enhanced light-matter interaction in a hybrid photonic-plasmonic resonator,” *Phys. Rev. A*, vol. 85, 2012, Art. no. 031805.
- [12]C. Ciminelli, D. Conteduca, F. Dell’Olio, and M. N. Armenise, “Design of an optical trapping device based on an ultra-high Q/V resonant structure,” *IEEE Photon. J.*, vol. 6, no. 6, Dec. 2014, Art. no. 0600916.
- [13]D. Conteduca *et al.*, “Rigorous design of an ultra-high Q/V photonic/plasmonic cavity to be used in biosensing applications,” *Opt. Laser Technol.*, vol. 77, pp. 151–161, 2016.
- A. O. Zaki, N. H. Fouad, D. C. Zografopoulos, R. Beccherelli, and M. A. Swillam, “Low-power compact hybrid plasmonic double-microring electro-optical modulator,” *Proc. SPIE*, vol. 9744, 2016, Art. no. 97441K.
  - B. Sun *et al.*, “Single-chip microprocessor that communicates directly using light,” *Nature*, vol. 528, pp. 534–538, 2015.
  - C. Guha, A. Gondarenko, and M. Lipson, “Minimizing temperature sensitivity of silicon Mach-Zehnder interferometers,”
- [14]*Opt. Exp.*, vol. 18, pp. 1879–1887, 2010.
- [15]S. Zhu, G. Q. Lo, and D. L. Kwong, “Electro-absorption modulation in horizontal metal-insulator-silicon-insulator-metal nanoplasmonic slot waveguides,” *Appl. Phys. Lett.*, vol. 99, 2011, Art. no. 151114.
- [16]A. O. Zaki, K. Kirah, and M.A. Swillam, “Hybrid plasmonic electro-optical modulator,” *Appl. Phys. A*, vol. 122, pp. 473–479, 2016.
- [17]M. Liu *et al.*, “A graphene-based broadband optical modulator,” *Nature*, vol. 474, pp. 64–67, 2011.
- [18]J.-S. Shin and J. T. Kim, “Broadband silicon optical modulator using a graphene-integrated hybrid plasmonic waveguide,”
- [19]*Nanotechnology*, vol. 26, 2015, Art. no. 365201.
- [20]V. J. Sorger, N. D. Lanzillotti-Kimura, R.-M. Ma, and X. Zhang, “Ultra-compact silicon nanophotonic modulator with broadband response,” *Nanophotonics*, vol. 1, pp. 17–22, 2012.
- [21]V. E. Babicheva, “Ultra-compact plasmonic waveguide modulators,” DTU FOTONIK, Dept. Photon. Eng., Tech. Univ. Denmark, Kongens Lyngby, Denmark, 2013.

- [22]M. Xu *et al.*, “Design of an electro-optic modulator based on a silicon-plasmonic hybrid phase shifter,” *J. Lightw. Technol.*, vol. 31, no. 8, pp. 1170–1177, Apr. 2013.
- [23]K. F. MacDonald and N. I. Zheludev, “Theoretical investigation of silicon MOS-type plasmonic slot waveguide based MZI modulators,” *Laser Photon. Rev.*, vol. 4, pp. 562–567, 2010.
- [24]C. Haffner *et al.*, “All-plasmonic Mach–Zehnder modulator enabling optical high-speed communication at the microscale,” *Nature Photon.*, vol. 9, pp. 525–528, 2015.
- [25]C. Lin, H. M. Wong, B. Lau, M. A. Swillam, and A. S. Helmy, “Efficient broadband energy transfer via momentum matching at hybrid junctions of guided-waves,” *Appl. Phys. Lett.*, vol. 101, 2012, Art. no.123115.
- [26]B. Lau, M. A. Swillam, and A. S. Helmy, “Hybrid orthogonal junctions: Wideband plasmonic slot-silicon waveguide couplers,” *Opt. Exp.*, vol. 18, pp. 27048–27059, 2010.
- [27]Lumerical Solutions, Inc., Vancouver, BC, Canada. 2003. [Online]. Available: <http://www.lumerical.com/tcad-products/fdtd/>
- [28]P. B. Johnson and R. W. Christy, “Optical constants of noble metal,” *Phys. Rev. B*, vol. 6, no. 12, pp. 4370–4379, 1973
- [29]J. Iverson *et al.*, “Electro-optic Pockels cell voltage sensors for accelerator diagnostics,” College Eng., Montana State Univ., Bozeman, MT, Canada, 2004.
- [30]S. Michel, J. Zyss, I. Ledoux-Rak, and C. T. Nguyen, “High-performance electro-optic modulators realized with a commercial side-chain DR1-PMMA electro-optic copolymer,” in *Proc. SPIE, Int. Soc. Opt. Photon.*, 2010, Art. no. 75990I.
- [31]D. A. B. Miller, “Device requirements for optical interconnects to silicon chips,” *Proc. IEEE*, vol. 97, no. 7, pp. 1166–1185, Jul. 2009

# Chapter 4: NEGATIVE & POSITIVE DISPERSION ENGINEERING IN MID- INFRARED REGION FOR HYBRID PLASMONIC WAVEGUIDE

## ABSTRACT

This study analyzes the dispersion properties of hybrid plasmonic waveguide in the mid infrared region, with both its negative and positive parts, using GaAs, AlAs and doped InAs as the materials for the three layers of the waveguide. The dispersion curve is engineered by changing the waveguide dimensions, and the doping level of the InAs. doping levels ranging from  $5E19 \text{ cm}^{-3}$  to  $2.5E20 \text{ cm}^{-3}$  are studied. Dimensions ranging from 150 nm to 4  $\mu\text{m}$  for the width of the waveguide, 150 nm to 3  $\mu\text{m}$  for the height of the cladding, and 10 nm to 100 nm for the height of the core are studied. It is observed that increasing the doping level, increases the slope of the negative dispersion part. Also the doping level has the ability to shift the dispersion curve with respect to the wavelength axis. All the dimensions have the ability to shift the dispersion curve with respect to the effective index axis.

**Keywords:** negative dispersion, mid infrared, hybrid plasmonic waveguide, semiconductors, plasmonics, dispersion curve engineering.

## INTRODUCTION

Plasmonics showed an advantage in manipulating light over previous technologies in last years, it showed an ability to confine light in sub-wavelength dimensions. This helped in Nano-scale integration of photonic devices to build better communication systems inter and intra electronic chips. Also in sensing applications, plasmonics helped in reaching higher sensitivity values. The interaction between the material to be sensed and the confined light is higher than non-plasmonic sensing mechanisms involving light.

Although plasmonics has this great advantage, many work is needed to engage plasmonics in different applications at cost effective and reliable way. Mid infrared region (MIR) is the range of choice for this work. Mid infrared region has a lot of potential in many applications. First, it contains the absorption



resonances of many molecules, this enables us to build chemical sensors in this region, which can aid in measuring environmental conditions, and in the diagnosis of certain diseases. Second, hot body radiations absorption bands are in the MIR, so this region can contribute to the security applications. Lastly, it can help in guiding light in quantum cascaded based laser systems (1-4).

To build any of these applications, first of all the waveguides in this range of wavelengths should be studied, as it forms the building blocks for any of these applications. In this study, the hybrid plasmonic waveguide is studied. The fabrication of this waveguide is straightforward with the normal masking, photolithography, etching and deposition steps. A negative and positive dispersion are observed in the waveguide, and the effect of the waveguide dimensions and doping levels on the dispersion curve are presented in this study. Since quantum cascade laser is the appropriate type of lasers used in mid infrared region, and these lasers are made by using InGaAs/AlInAs alloys on InP and GaAs/AlGaAs on GaAs in this wavelength range (2,5). InAs, GaAs and AlAs were chosen to be our building materials for the waveguide, so that complete systems can be easily built using the same fabrication technology.

The chapter is organized as follows, the second section presents the structure of the waveguide, and the material models used. The third section presents the dispersion analysis results, and the effect of the dimensions and doping level on the shape of the dispersion curve. the last section is the conclusion.

## 4.1 OVERVIEW AND MATERIAL MODELING

The hybrid structure is shown in Figure 4-1, it is a three layer waveguide built on GaAs substrate, the upper layer is N-doped InAs, the middle layer is AlAs, and the bottom layer is GaAs, and the waveguide is surrounded by air. Constant real epsilons were used for the GaAs and AlAs, 3.283 for GaAs and 2.84 for AlAs (6).

For the n doped InAs, the Drude model is used:

$$\varepsilon(\omega) = \varepsilon_s \left( 1 - \frac{\omega_p^2}{\omega^2 + \Gamma^2} \right) + i\varepsilon_s \left( \frac{\Gamma \cdot \omega_p^2}{\omega(\omega^2 + \Gamma^2)} \right)$$

This model shows the dependence of the relative permittivity of any material containing a lot of free carriers, on the frequency of the flowing EM fields in the material, the relative permittivity also depends on the permittivity of the pure InAs  $\varepsilon_s$ , the plasma frequency  $\omega_p$ , and the scattering rate of the carriers  $\Gamma$ . The plasma frequency is given by:

$$\omega_p^2 = \frac{ne^2}{\varepsilon_s \varepsilon_0 m^*}$$

it depends on the free carrier density  $n$ , which is the doping level in this case, the electronic charge  $e$ , the permittivity of the free space  $\varepsilon_0$ , and the effective mass of the free carriers in the material  $m^*$ . One of the scattering mechanisms that affects the mobility of the free carriers is the ion scattering, this phenomena makes the mobility of the free carriers function in the doping level, in turns the effective mass and the scattering rate are functions in the doping level (7). The effective mass is related directly to material parameters through (7):

$$m^* = \left( \frac{h^2}{2\Delta E_g n} \right) \left( \frac{3n}{8\pi} \right)^{2/3}$$

where  $h$  is plank's constant,  $n$  is the doping level, and  $\Delta E_g$  is the band gap narrowing. The band gap narrowing is related to the doping level through (8):

$$\Delta E_g = A \cdot n^{1/3} + B \cdot n^{1/4} + C \cdot n^{1/2}$$

where  $A$ ,  $B$  and  $C$  are constants, for InAs they are determined to be  $14 \times 10^{-9}$ ,  $1.97 \times 10^{-7}$  and,  $57.9 \times 10^{-12}$  respectively (8).

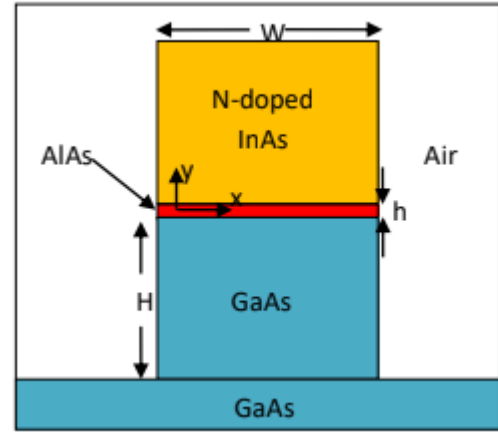


Figure 4-1 the hybrid plasmonic waveguide, labeled with the materials used, symbols for dimensions and the axes direction and position.

The scattering rate is related to effective mass and mobility through:

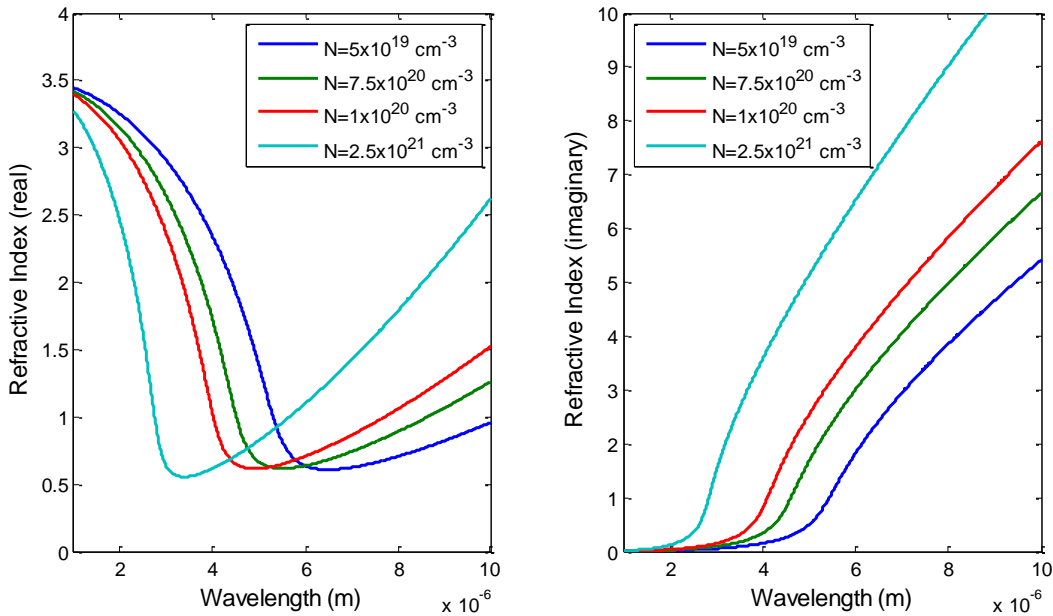
$$\Gamma = \frac{e}{\mu m^*}$$

where the hall mobility is represented by the empirical model (9):

$$\mu(N) = \mu_{min} + \frac{\mu_{max} \left( \frac{300}{T} \right)^{\theta_1} - \mu_{min}}{1 + \left( \frac{N}{N_{eff} \left( \frac{T}{300} \right)^{\theta_2}} \right)^\lambda}$$

where T is the temperature (300 K), and the other parameters are fitted to the experimental data in (7), the  $\mu_{max}$ ,  $\mu_{min}$ ,  $\theta_1$ ,  $\theta_2$ ,  $N_{eff}$  and  $\lambda$  equals 35400, 80, 1.57, 3,  $1.8E17$ , 0.86 respectively. The mobility is related to the hall mobility through the hall factor, which equals 1 for the InAs for doping levels higher than  $1E19 \text{ cm}^{-3}$  (10). The relative permittivity and refractive index of the InAs are shown in Figure 4-2.

Lastly in this section, finite element method is used throughout this analysis, and 10 elements per feature are used as a minimum for meshing following the rule of thumb.



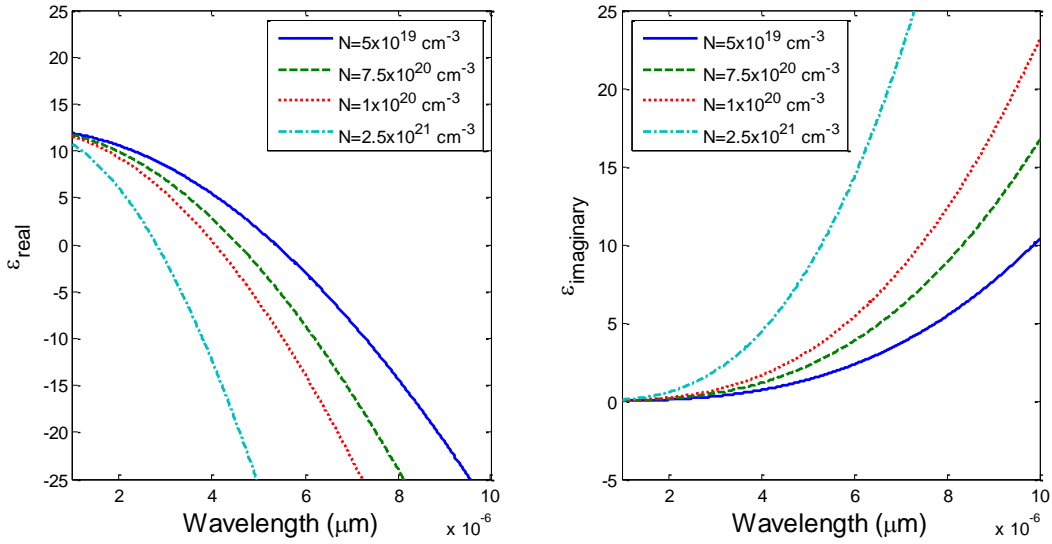


Figure 4-2 shows the real and imaginary parts of the refractive index (upper curve). shows the real and imaginary parts of the relative permittivity (lower curve).

## 4.2 RESULTS & DISCUSSION

In this section, the results of this study will be discussed. First, the modal shapes and dispersion curves are presented, and the effect of the waveguide dimensions and doping ( $n$ ) are discussed then. As can be seen in Figure 4-3, the dispersion curve is divided into two main parts. At higher wavelengths, the modal shape is a normal hybrid plasmonic mode. While at lower wavelengths, negative dispersion appears, and more field moves inside the InAs. The field is partially confined in the InAs at the epsilon near zero (ENZ) of the doped InAs.

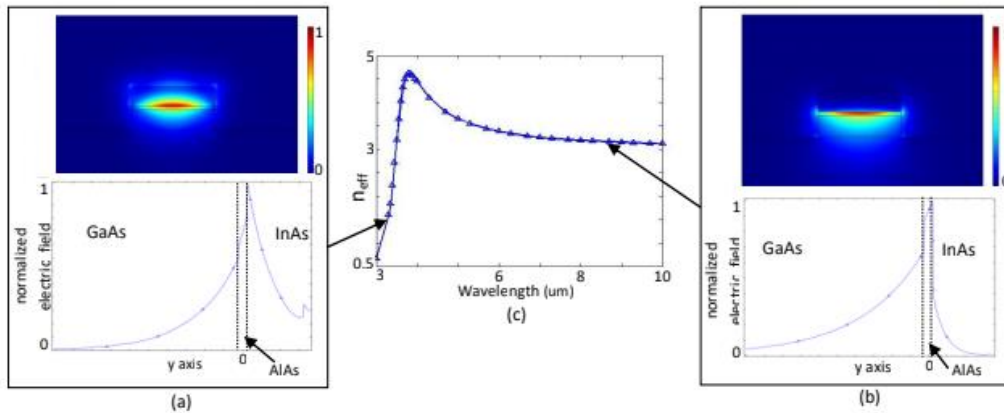


Figure 4-3 fig(3a) shows the surface plot and 1D plot of the modal shape at wavelength equals 3.3  $\mu\text{m}$ , fig(3b) at wavelength equals 8  $\mu\text{m}$ , and fig(3c) shows a dispersion curve, all are at doping =  $2.5E20 \text{ cm}^{-3}$ ,  $W = 2 \mu\text{m}$ ,  $H = 0.6 \mu\text{m}$ , and  $h = 100 \text{ nm}$ . The 1D plots are taken at the white dashed lines in the surface plot.

Figure 4-4 shows how the mode transforms as the wavelength increase, note the AlAs is a 100 nm layer around zero in the graph. it can be observed that the confinement of the field decreases with the wavelength decrease. Also, the losses increase due to the increased number of free carriers in the doped InAs region.

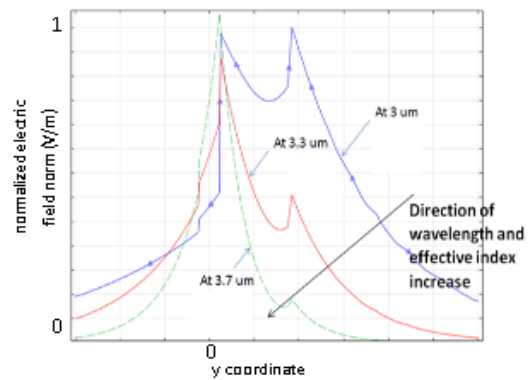


Figure 4-4 Modal shapes taken at the dashed white line in the above surface plot.

Figure 4-5 shows the effect of the doping on the modal shape, it is observed from the graph that increasing the doping level causes an increase in the confinement of the mode from the side of the InAs (positive side of the graph), and this is intuitive to understand, as the higher free carriers absorb the field faster, while the confinement decreases from the GaAs side, (the negative part of the graph). This is intuitive to understand. The higher free carrier concentration absorbs the field faster, while the confinement decreases from the GaAs side, (the negative part of the graph).

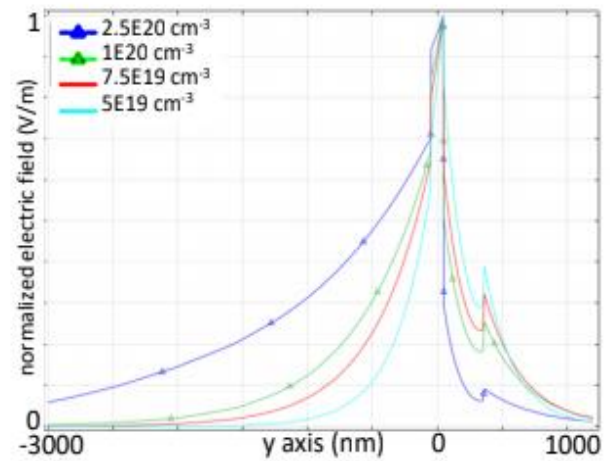


Figure 4-5 The modal shapes of the plasmonic modes at different doping, all are at wavelength = 7.5  $\mu\text{m}$   $W = 2\mu\text{m}$ ,  $H = 0.3\mu\text{m}$ .

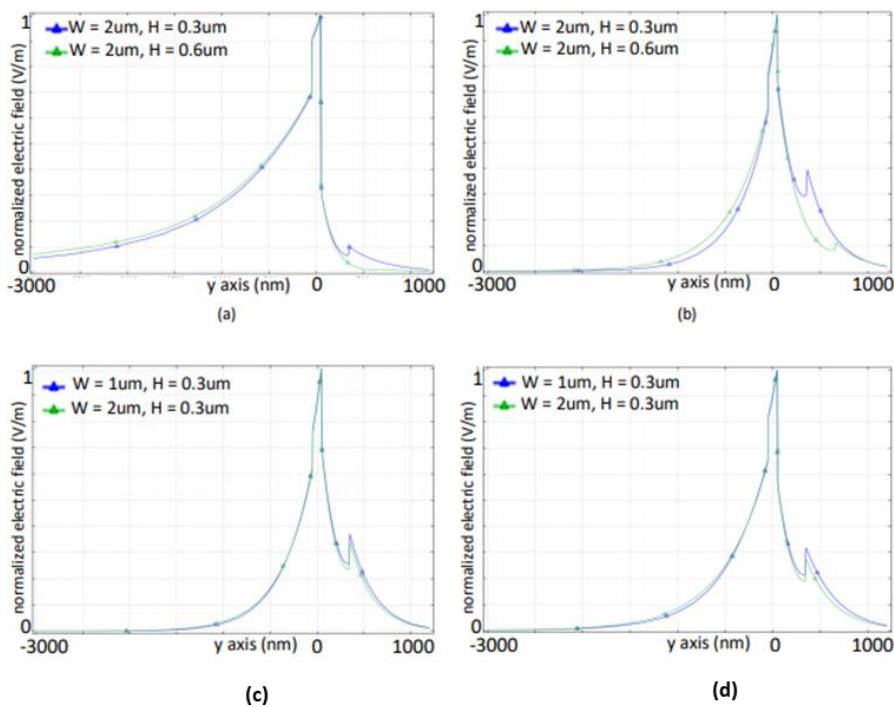


Figure 4-6 shows the modal shapes at different dimensions. fig(6a) is at doping equals  $2.5E20\text{ cm}^{-3}$  , wavelength equals 7  $\mu\text{m}$ , fig(6b) is at doping equals  $5E19\text{ cm}^{-3}$  , wavelength equals 8  $\mu\text{m}$ , fig(6c) is at doping equals  $7.5E19\text{ cm}^{-3}$  , wavelength equals 7  $\mu\text{m}$ , fig(6d) is at doping equals  $1E20\text{ cm}^{-3}$  , wavelength equals 7  $\mu\text{m}$ .

Figure 4-6, shows the effect of the waveguide dimensions including H & W on the modal shapes, generally, it can be observed that these dimensions have little effect on the modal shapes. Figure 4-5(a & b) show the effect of varying the clad height, as the height increases from 0.3  $\mu\text{m}$  to 0.6  $\mu\text{m}$ , the confinement of the field decreases from the GaAs side, so smaller amount of power is left on the InAs part, this makes the jump of the field due to the boundary conditions at the InAs-air interface smaller, in addition to the fact that this jump occurs after the field travels more in the InAs due to the larger height, so the confinement increases at the InAs side.

Figure 4-6 (c&d) show the effect of the clad width on the modal shapes. This parameter has even smaller effect, as the width increases from 1  $\mu\text{m}$  to 2  $\mu\text{m}$ , the confinement slightly decreases on the GaAs side and increases on the InAs side.

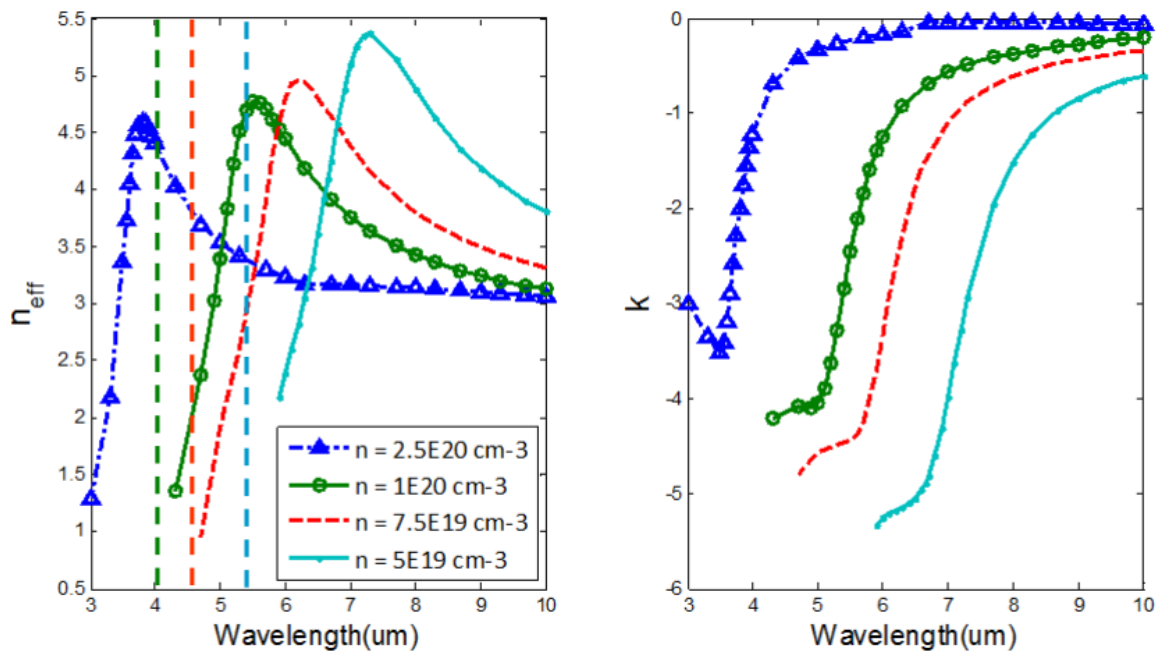


Figure 4-7 The effective mode index ( $n_{\text{eff}}$ ) and the extension coefficient ( $k$ ) at various doping ( $2.5E20 \text{ cm}^{-3}$ ,  $1E20 \text{ cm}^{-3}$ ,  $7.5E19 \text{ cm}^{-3}$ ,  $5E19 \text{ cm}^{-3}$ ). The vertical dashed lines mark the position of the plasma wavelength, the green line, the red, and the cyan line are for  $1E20 \text{ cm}^{-3}$ ,  $7.5E19 \text{ cm}^{-3}$ ,  $5E19 \text{ cm}^{-3}$  doping respectively. The plasma wavelength of the  $2.5E20 \text{ cm}^{-3}$  is below 3  $\mu\text{m}$ .

Moving to the dispersion curves. In Figure 4-7, the dispersion curves at various doping of the InAs are shown ( $5E19\text{ cm}^{-3}$ ,  $7.5E19\text{ cm}^{-3}$ ,  $1E20\text{ cm}^{-3}$  &  $2.5E20\text{ cm}^{-3}$ ). As the doping increases, the dispersion curve is affected in several ways. First, the dispersion curve is shifted up. Second the plasma frequency and the peak of the dispersion curve are shifted towards lower wavelengths, leaving a wider bandwidth for the hybrid plasmonic mode. Third, the wavelength range where negative dispersion can be obtained is shifted down. Lastly, the slope of the negative dispersion part increases. Also increasing the doping level, decreases the losses of the hybrid plasmonic mode, as it becomes further from the plasma frequency.

Figure 4-8 is a group of curves that shows the effect of the dimensions and doping on the dispersion curve, from which the different trends can be interpreted. The real part will be discussed first, by looking at Figure 4-8 (a) at the inset of the doping  $2.5E20\text{ cm}^{-3}$ , we can get several conclusions. First, increasing the width of the waveguide ( $W$ ), causes an increase in the effective index of the positive dispersion region. On the other hand, it approximately has no effect on the negative dispersion.



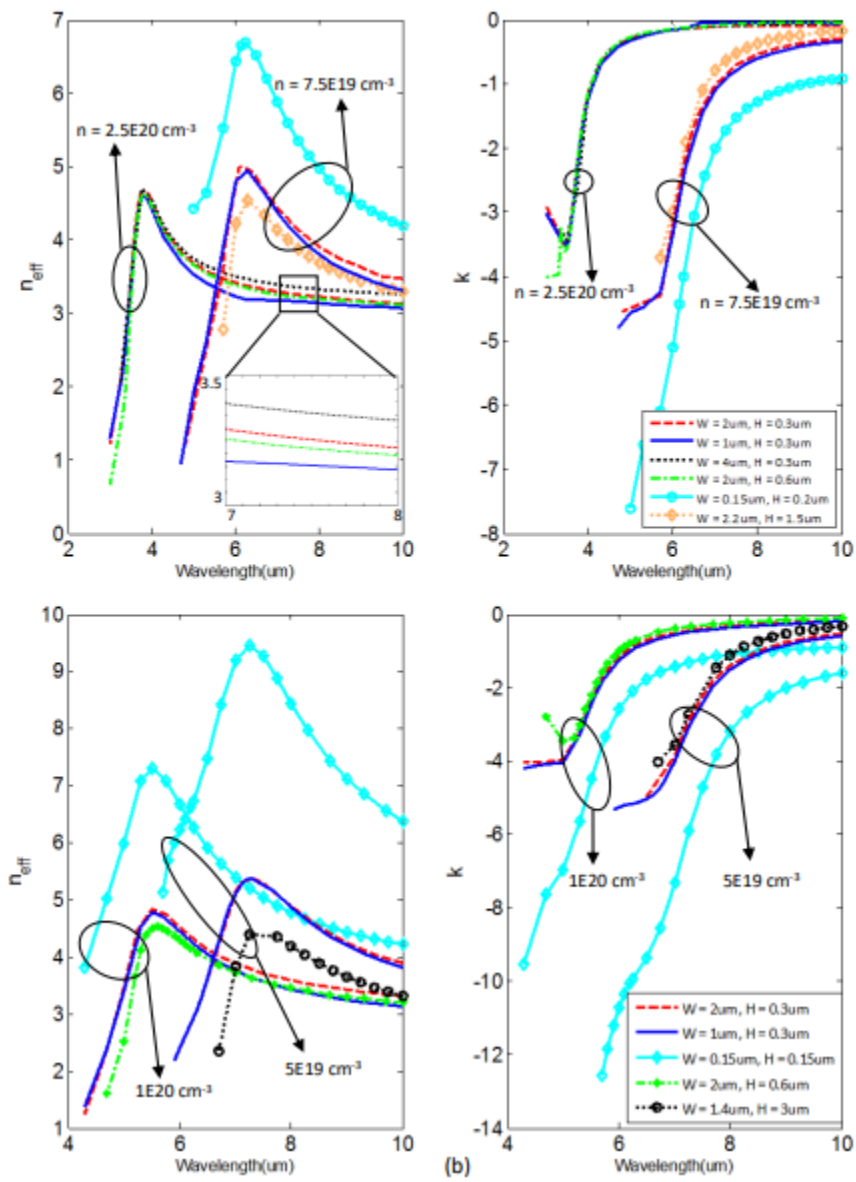


Figure 4-8 shows dispersion curves at doping levels, and different widths and heights, for the waveguide, at constant core height, which is equal to 100 nm.

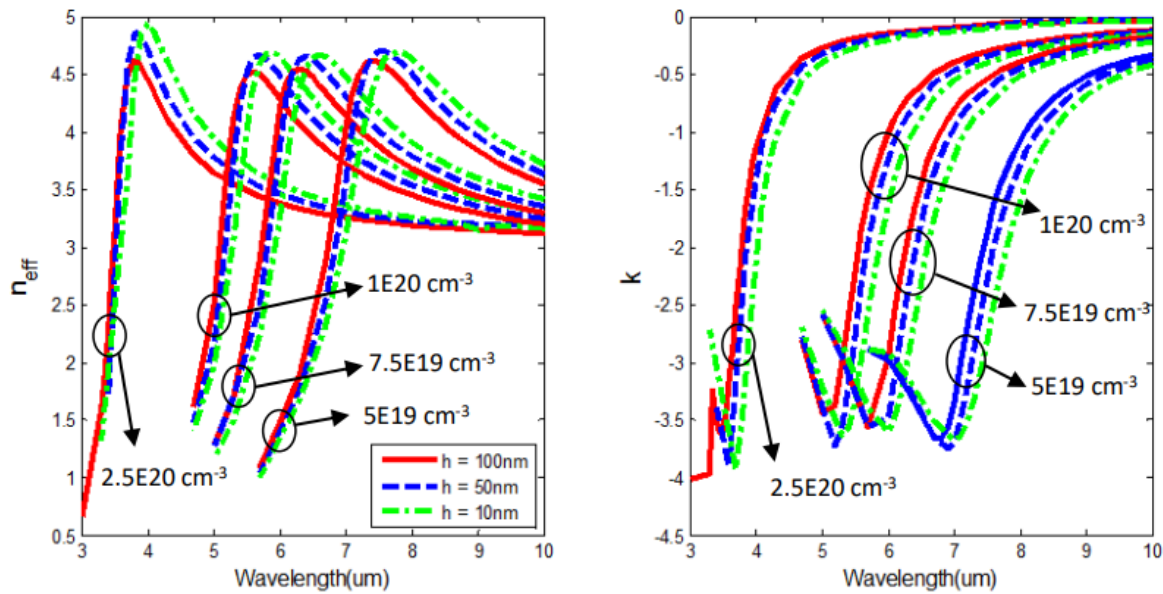


Figure 4-9 shows dispersion curves at different core heights ( $h$ ), at different doping levels, all the curves are at waveguide width equal to 2  $\mu\text{m}$ , and height equal to 0.6  $\mu\text{m}$ .

Second, increasing the height of the cladding ( $H$ ) has an opposite effect. a decrease in the effective index of the hybrid mode in the positive dispersion region occurs, and slightly increases the slope of the negative dispersion region. by looking at the dispersion curves at the other doping levels, the same observation can be made. In the group of graphs regarding the doping level  $5\text{E}19 \text{ cm}^{-3}$  Figure 4-8 (a), there is a dispersion curve at dimensions equal to 150 nm width ( $W$ ) and 150 nm height ( $H$ ). This dispersion curve is shifted upward a lot higher than the other curves, it is concluded that the dispersion curve is a stronger function in height. The same conclusion can be reached by looking at the other dimensions.

For the imaginary part, as the area of the waveguide increases, the losses decreases, which means that the absolute value of the imaginary part decreases, and this is easy to understand, as the field confines in a smaller area, more field flows in the doped InAs, which causes higher losses. Now, let's move to Figure 4-9, where the effect of the height will be investigated of the core. The conclusion is simple, as the height of the core ( $h$ ) increases, the peak of the curve increases. Also, the slope of the negative dispersion part increases, and the absolute value of the slope in the positive part increases. All these effects are stronger at lower doping levels.

### 4.3 CONCLUSION:

Using doped semiconductors enables us to control the plasma frequency to the mid infrared region, while keeping fabrication simple. The negative dispersion properties of this waveguide will enable it to enter a new category of applications. III-V media can help in building complete systems including source, detector and guiding using the same technology.

### REFERENCES

- [1] Plasmonic waveguides in Mid infra-red using silicon-insulator-silicon. SPIE OPTO: International Society for Optics and Photonics; 2015.
- [2] Stanley R. Plasmonics in the mid-infrared. *Nature Photonics* 2012;6(7):409-411.
- [3] Law S, Podolskiy V, Wasserman D. Towards nano-scale photonics with micro-scale photons: the opportunities and challenges of mid-infrared plasmonics. *Nanophotonics* 2013;2(2):103-130.
- [4] Li D, Ning C. All-semiconductor active plasmonic system in mid-infrared wavelengths. *Optics express* 2011;19(15):14594-14603.
- [5] Yao Y, Hoffman AJ, Gmachl CF. Mid-infrared quantum cascade lasers. *Nature Photonics* 2012;6(7):432-439.
- [6] Palmer C, Stavrinou P, Whitehead M, Phillips C. Mid-infrared ( $\lambda \sim 2\text{--}6 \mu\text{m}$ ) measurements of the refractive indices of GaAs and AlAs. *Semiconductor science and technology* 2002;17(11):1189.
- [7] Law S, Adams D, Taylor A, Wasserman D. Mid-infrared designer metals. *Optics express* 2012;20(11):12155-12165.
- [8] Jain S, McGregor J, Roulston D. Band-gap narrowing in novel III-V semiconductors. *J Appl Phys* 1990;68(7):3747-3749.
- [9] Sotoodeh M, Khalid A, Rezazadeh A. Empirical low-field mobility model for III-V compounds applicable in device simulation codes. *J Appl Phys* 2000;87(6):2890-2900.
- [10] Popovic RS. Hall effect devices. : CRC Press; 2003.



# Chapter 5: MID-INFRARED III-V ELECTRO-ABSORPTION HYBRID PLASMONIC MODULATOR

Abstract:

An electro-absorption modulator in midinfrared region, built on hybrid plasmonic waveguide concept, using III-V media is proposed in this work.

## 5.1 INTRODUCTION

Midinfrared range of wavelength is rich of possibilities, it has the electromagnetic footprint of many hazardous molecules and many biological elements which makes it ideal for sensing applications [1][2]. Also, it has a low loss windows in the midinfrared region, which makes it suitable for free space communication [2]. Expanding the telecommunication wavelength range to higher than 2  $\mu\text{m}$  is one motivation for such research [3]. Also, longer wavelengths can be utilized in free-space communications modulator, signal processing and switching applications [4].

The light sources used in midinfrared region is Quantum cascade lasers, due to its high efficiency [5]. These laser sources, are built based on III-V semiconductor media. Consequently, building other optical components using the same technology, opens the door for complete integrated systems being built on the same technology, without the need to couple from or to silicon on insulator technology, including, light sources [5][11][12][13][14][15], modulators, sensors [6][7][8][9], and detectors [10]. Also, this platform enables working at higher wavelength range [11], and it opens the doors for design capabilities that is beyond the SOI platform, due to the III-V material's superior electronic properties [11].

One of the components that is needed for optical sensor photonic circuits, is optical modulators. For experimental characterization of midinfrared components, a combination of a chopper and lock in amplifier is often used to increase the signal to noise ratio, whose purpose is to shift the system to a higher frequency, where frequency dependent noise is smaller. An optical modulator could replace the chopper in an on-chip system [16].

Few groups tried to work on midinfrared modulators by extending the Si or Ge based modulators to the midinfrared region [17][18]. SOI carrier injection modulators with speed up to 3 Gb/s at 2165 nm

wavelength [19], and GOI modulators at 1950 nm wavelength [20] have been demonstrated. An MZI-based PN junction modulator in the SOI platform has been demonstrated at 1950 nm. The device operates at carrier depletion mode, a modulation efficiency of 2.02 V.cm at 1550 nm and 2.68 V.cm were measured. An open eye diagram at 20 Gb/s with a 5.8 dB extinction ratio were measured.

As it is clear from this short summary of Si and Ge based midinfrared modulators, structures are still having a very big footprint, and high insertion losses which is not suitable for working in Lap-On-Chip applications. Few studies tried to exploit the capabilities of plasmonics in midinfrared optical modulators. Hybrid plasmonic waveguides have many advantages. They utilize the plasmonic feature of highly confining light in subwavelength dimensions from one side, allowing for higher ability to control light, while it is easier to couple light to and from it [21]. In this study, we present a plasmonic modulator that is based on the hybrid plasmonic waveguide presented in the previous chapter.

This chapter goes on as follows, first the modulator principle is discussed in section 2. The design process is divided to three sections, in section 3, electrical behavior of the modulator is discussed. In section 4, modal analysis of the optical modes is discussed. From this stage a primary design dimensions and materials was determined. In section 4, complete electromagnetic simulations using finite difference method is presented, and the modulator performance parameters are discussed. Section 5 is the conclusion.

## 5.2 MODULATOR PRINCIPLE

The modulator is based on a hybrid plasmonic waveguide [21], that is built on a GaAs substrate, as shown in Figure 5-1 (a). The waveguide consists of three layers; The upper layer is a Doped InAs that is used as the plasmonic material. The doped InAs model is the same as the one used in the previous chapter. The core material and InAs doping levels are optimized for the highest possible extinction ratio, and the bottom material is GaAs. GaAs/AlGaAs platform is used to be the power feeding optical waveguides in the modulator and out of the it. The Al content in the AlGaAs layer is optimized for the highest possible coupling to the hybrid plasmonic waveguide.

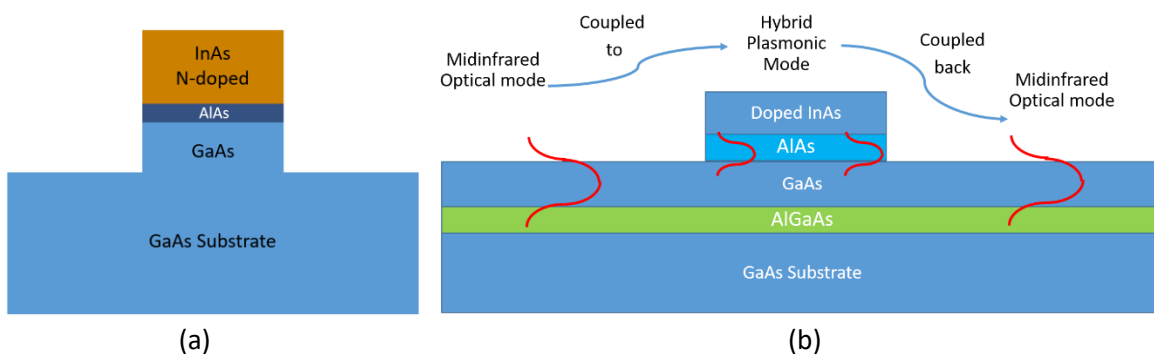


Figure 5-1, to the left (a), the hybrid plasmonic waveguide built on a GaAs substrate is shown. To the right (b), the modulator schematic shows the mode coupling from the GaAs/AlGaAs optical waveguide to the hybrid plasmonic waveguide, and then back to the optical waveguide.

The modulator structure is shown in Figure 5-1(b). The optical fundamental TM mode propagates in the GaAs/AlGaAs optical waveguide. The optical power is partially coupled to the hybrid plasmonic waveguide, constituting a four-layer mode -InAs/AlAs/GaAs/AlGaAs- which is named the coupled mode. This mode's power is shared between the hybrid plasmonic mode and the optical mode. It propagates through the modulator, where it experiences losses from the plasmonic part of the coupled mode. The remaining coupled mode's power in the hybrid plasmonic waveguide couples back to the optical mode at the end of the modulator length. Some losses occur at the end of the modulator from field scattering due to the mismatch between the end of the plasmonic waveguide and the optical waveguide.

The Hybrid plasmonic waveguide acts as a PIN diode from the electrical point of view, so that the carrier concentration in the InAs can experience changes as a response to electrical signals. Consequently, the

dispersion properties of the hybrid plasmonic mode is controlled, creating the ability to manipulate the flowing power. In the off state, the losses of the hybrid mode are tuned to be high, consequently most of the power gets lost. In the on state, at the end of the modulator length, the hybrid mode gets coupled back to the optical waveguide, while some of the power gets scattered.

### 5.3 CHARGE SIMULATIONS

In order to quantify the ability of the structure to accumulate charge or deplete charge, charge simulations are done using Device Lumerical simulator. The simulator solves Poisson's equation and the drift-diffusion equations simultaneously. The electrical models for the materials are used from the program's own library, the models contain the material's energy bands parameters, mobility as a function doping models, effective mass data, and different recombination models. Meshing was chosen such that no part of the structure has less than 10 mesh elements, and meshing convergence test were carried out to ensure that the simulations are not mesh dependent.

The structure used is shown in Figure 5-2, the structure resembles a PIN diode, where InAs is the n-region, AlAs is the intrinsic region and GaAs is a lightly doped region, where P-doping of  $1E14 \text{ cm}^{-3}$  is added to the whole GaAs waveguide. GaAs rib waveguide is used instead of strip waveguide, so as to be able to add Aluminum contacts as shown, to electrically connect GaAs to the electrical ground of the control electronic circuit. Another Aluminum contact is added on top of the doped InAs, to carry the control electrical signal. The rest of the structure is the same as discussed in the previous section.



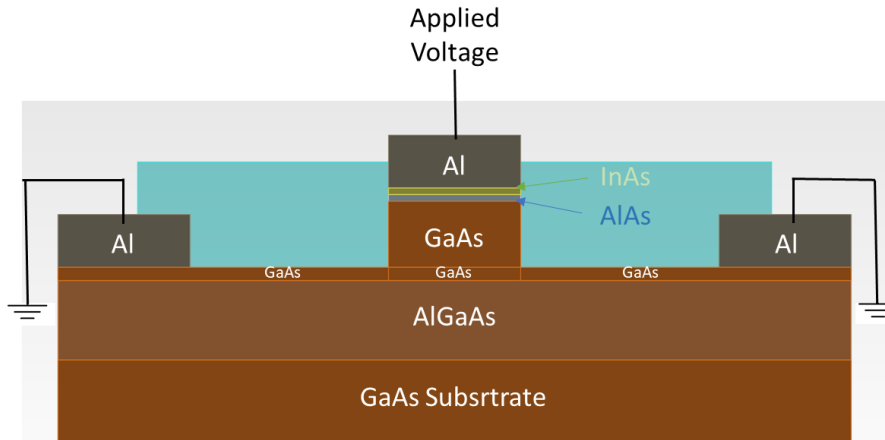


Figure 5-2, the modulator design showing the GaAs substrate, the AlGaAs buffer layer, then the GaAs rip waveguide, then the Hybrid plasmonic AlAs and doped InAs layers, and the Aluminum contacts for electrical control.

At first the possibility of depleting the carriers from the n-doped InAs layer is studied. Using the dispersion curves of the hybrid plasmonic waveguide discussed in the previous chapter (chapter 4), an initial doping of  $1E20 \text{ cm}^{-3}$ , so as to create a plasmonic effect at wavelength equal to and higher than  $5 \mu\text{m}$ . A positive voltage is applied to the top Aluminum contact to deplete the negative electrons in the InAs layer. No depletion is noted at all in the InAs layer, on the contrary the GaAs is nearly fully depleted, as shown in Figure 5-3. This occurs because the very high doping required for creating the plasmonic effect in the midinfrared region drives the InAs material into degeneracy due to its very small  $0.36 \text{ eV}$  band gap [26].

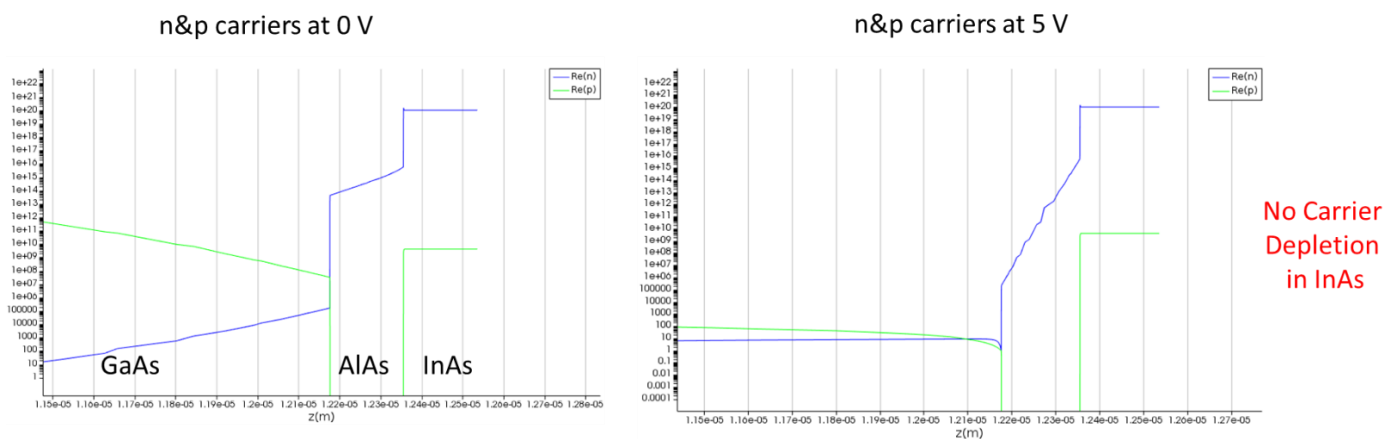


Figure 5-3, the charge distribution at 0 V and 5 V are shown to the left and right respectively.

Next, charge accumulation is studied instead of charge depletion, where the InAs is doped with a doping less than the required for the plasmonic effect at midinfrared operation. The applied voltage accumulates charges enough to allow for the hybrid plasmonic mode propagation in midinfrared region. Figure 5-4 shows the n and p curves to the side of the band diagram at 5 V. The charge is accumulated at the AlAs-InAs interface, which makes the charge increases from  $1E16 \text{ cm}^{-3}$  to  $7.7E18 \text{ cm}^{-3}$ .

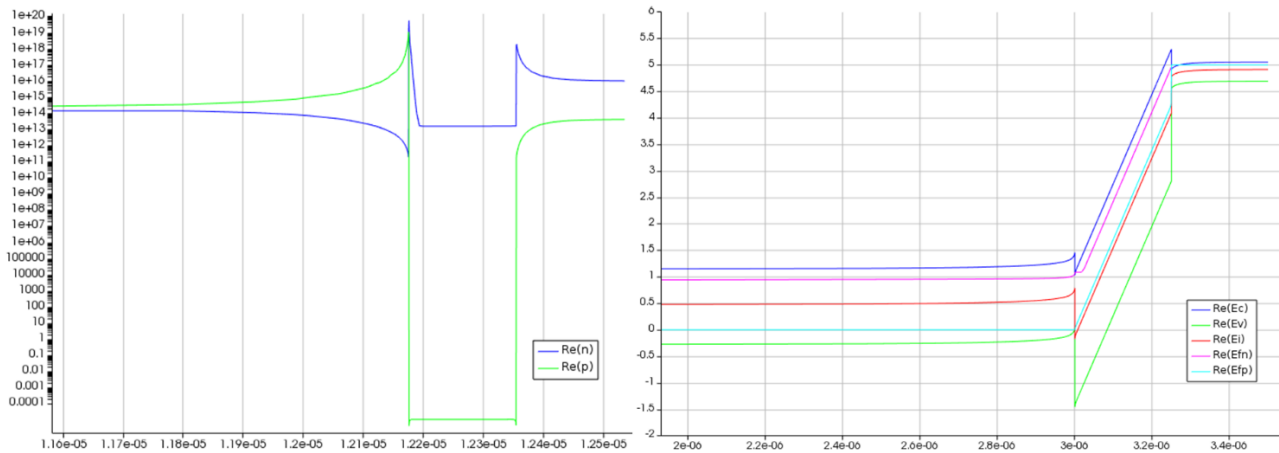


Figure 5-4, to the left is the charge distribution at -5V, showing the accumulation. To the right is the band diagram at the same voltage level.

The capacitance of the structure is studied as shown in Figure 5-5. At low enough doping levels (e.g.  $1E16 \text{ cm}^{-3}$  in this case), where the InAs is not degenerate, part of the depletion region of the PIN structure is in the InAs region. The capacitance of the structure is the highest at no voltage, as the voltage increases, and the intrinsic depletion region of the structure decreases, the capacitance of the structure decreases.

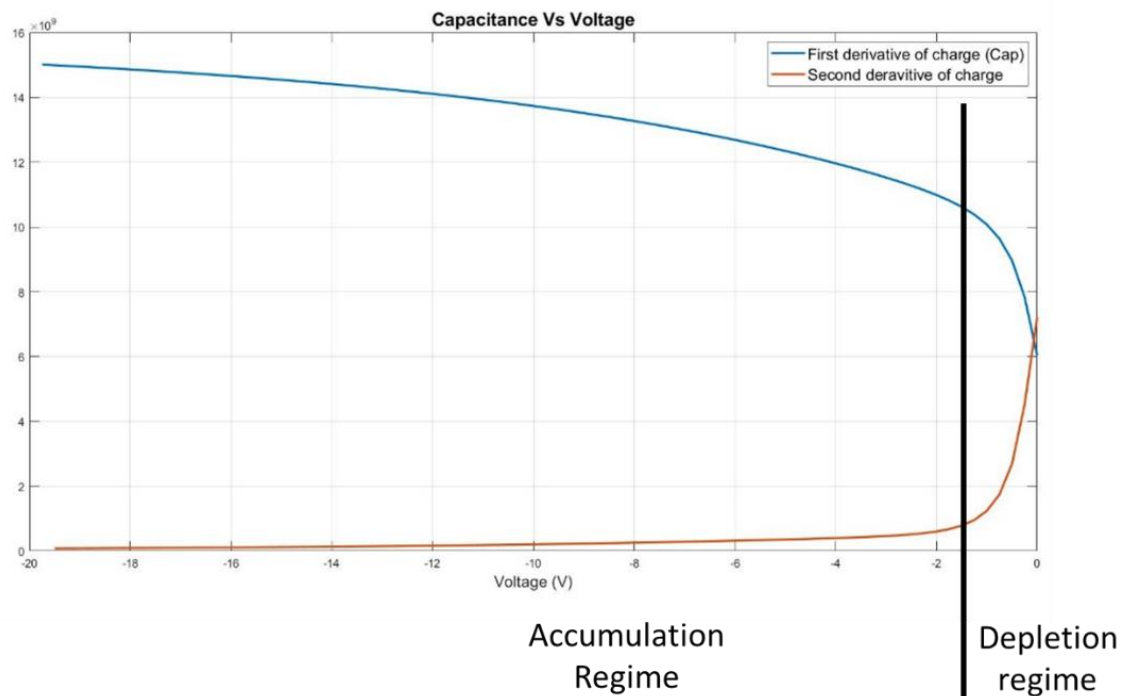


Figure 5-5, the AC capacitance of the modulator.

Superlattice had to be employed instead of the plain doped InAs layer, as to create many accumulation layers, as the single accumulation layer is not seen by the optical field as a doped region, while the field deals with the superlattice region as one doped region.

The superlattice is formed of ten InAs-AlAs layers, with InAs 10 nm high, and AlAs 5 nm high, as shown in Figure 5-6. The AlAs is chosen to be smaller than the InAs so as for the peaks of the charge to be nearly grouped. Based on the previous chapter, the base superlattice doping is chosen to be  $4E19 \text{ cm}^{-3}$ , where we are sure that there is no plasmonic mode at wavelengths in the range from  $3 \mu\text{m}$  to  $8 \mu\text{m}$ , and then biasing voltage raises the charge to allow for the propagation of the plasmonic mode in target wavelength range. The charge distribution is shown in Figure 5-7. The charge level at any of the InAs layers in Figure 5-7 is  $6.7E19 \text{ cm}^{-3}$  at 5 V.

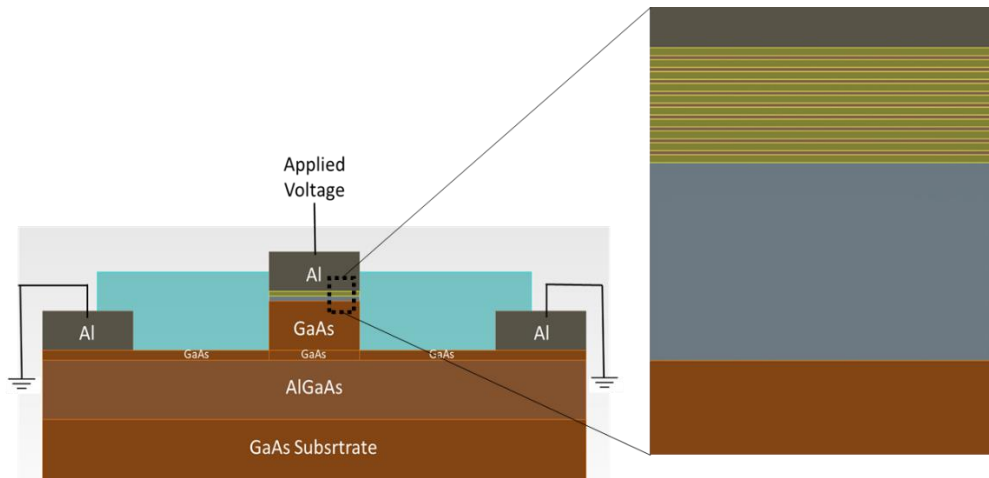


Figure 5-6, the modulator design with the superlattice.

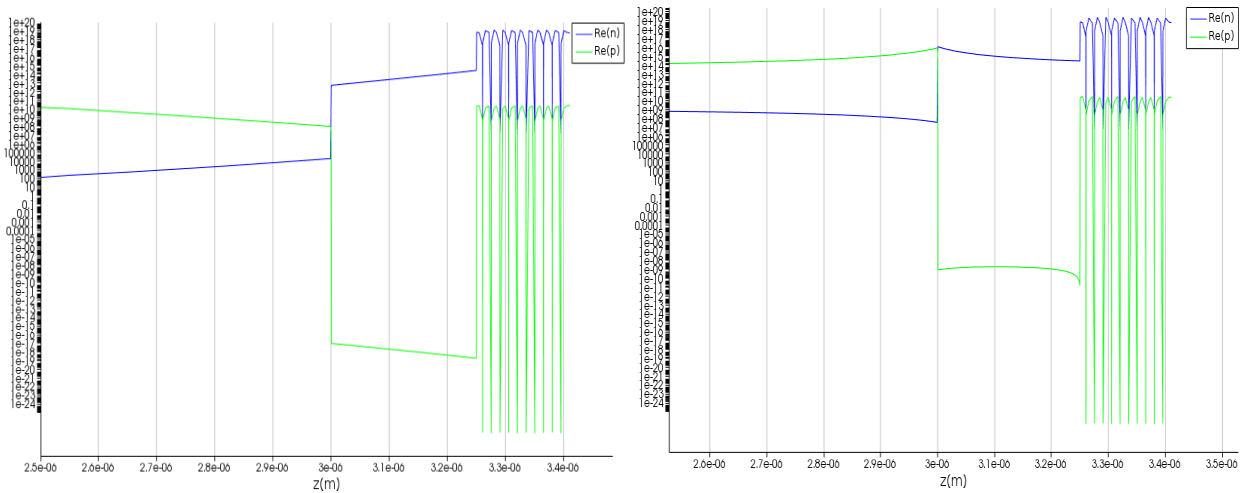


Figure 5-7, the charge distribution in the modulator. To the left is at no voltage. To the right is at -5 V.

As the applied voltage increases from 0 to 20 V, the charge increases from the base  $4E19 \text{ cm}^{-3}$  to  $1.5E20 \text{ cm}^{-3}$ , which is an appropriate charge level as will be seen later in the modal analysis section for the wavelength range from  $4 \mu\text{m}$  to  $8 \mu\text{m}$  (next section), Figure 5-8. It is worth mentioning that, lower doping should be used in case of working at higher wavelength range; consequently, higher voltage levels will be needed accumulate enough charge to work at lower wavelength ranges. Note that the voltage is normalized in this graph, while the actual applied voltage is negative.

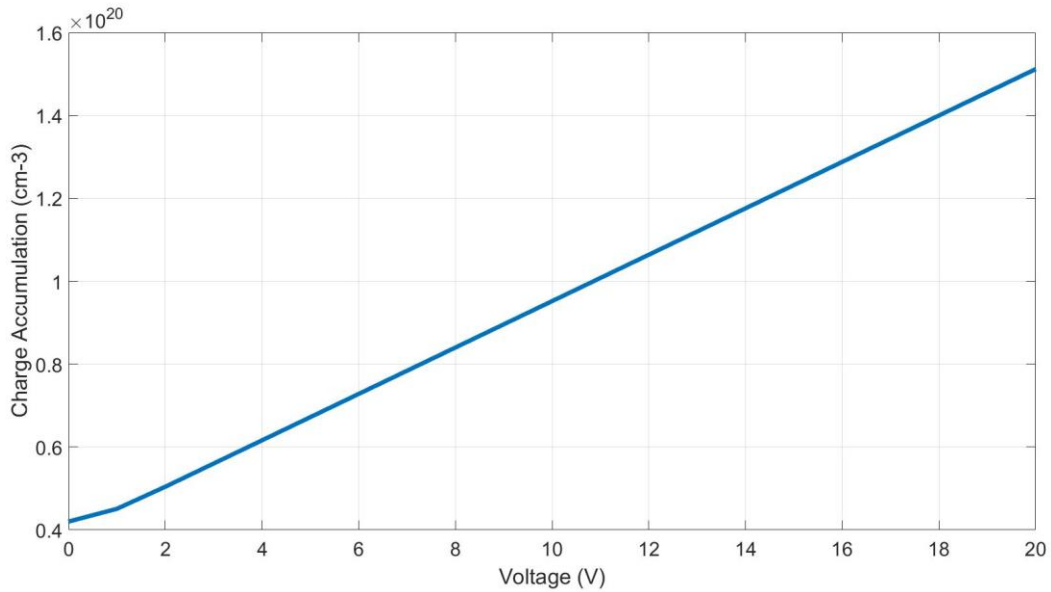


Figure 5-8, The charge accumulation in any of the InAs layers in the superlattice vs the voltage.

A 2D Finite Difference Time Domain (FDTD) simulation (FDTD simulations will be discussed in section 5.5 in details) is shown in Figure 5-9, to show the modulator transmission with and without superlattice in the low power state, it is clear that without a superlattice, the modulator is transparent from 4 um to 10 um wavelength. While with superlattice structure, there is a significant decrease in transmission, which will be optimized and discussed later on.

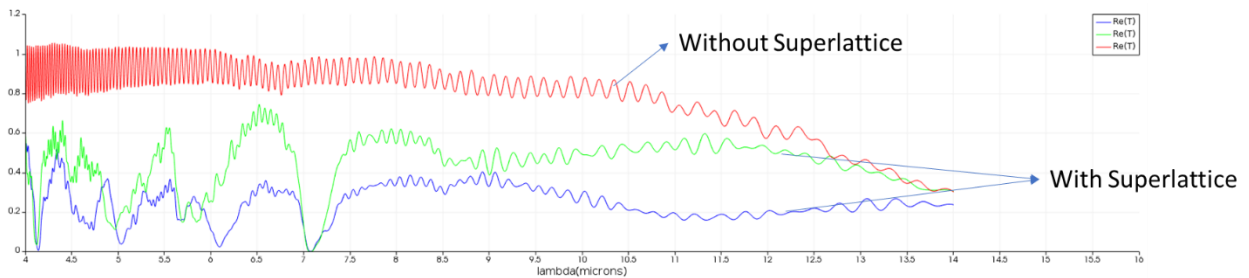
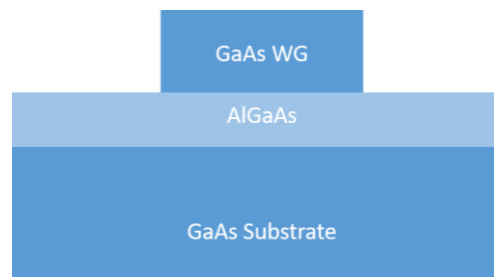


Figure 5-9, FDTD transmission of the modulator with and without a superlattice.

## 5.4 MODAL ANALYSIS:

The modal analysis presented in this section is done on Mode Solutions Lumerical simulator. Meshing, boundary conditions were optimized to ensure simulator accurate results. Two groups of dispersion curves are calculated and discusses, modal analysis of the optical waveguide (shown in *Figure 5-10, the GaAs/AlGaAs optical waveguide.*), and hybrid plasmonic modes incorporating the superlattice discussed previously.



*Figure 5-10, the GaAs/AlGaAs optical waveguide.*

Figure 5-11, dispersion curve of the hybrid plasmonic waveguide (from previous chapter), also the symmetric and antisymmetric modes are shown. shows the dispersion curves of the Hybrid plasmonic waveguide from the previous chapter. The dispersion curves showed that there are two modes for the waveguide, one is symmetric and the other is symmetric. Since the choice were made in this study to work with the fundamental mode of the optical waveguide, then we only consider the symmetric hybrid plasmonic mode in this study, as it is the one that can be coupled to the optical mode.

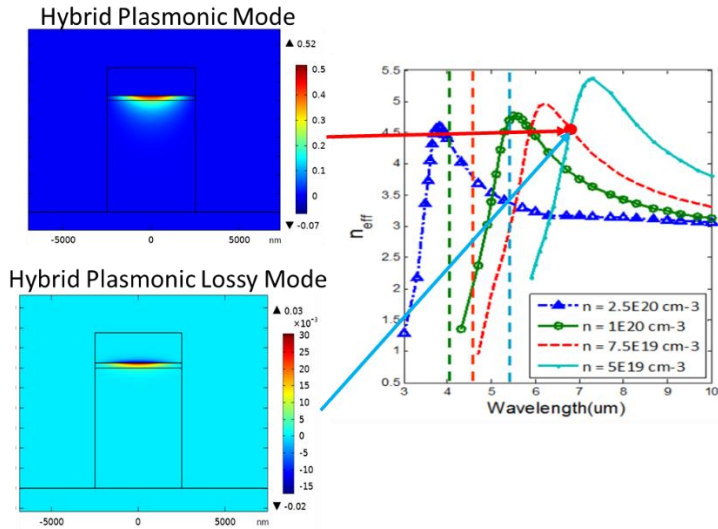


Figure 5-11, dispersion curve of the hybrid plasmonic waveguide (from previous chapter), also the symmetric and antisymmetric modes are shown.

First, effective media concept discussed in [27] is used to replace the superlattice with an equivalent material. The following equation is used [27]:

$$\epsilon_{eff} = f_1\epsilon_m + f_2\epsilon_d$$

Where  $\epsilon_m$  is the permittivity of the conductor, which is InAs in our case,  $\epsilon_d$  is the permittivity of dielectric, which is AlAs in our case.  $f_1$  and  $f_2$  are filling ratios, which is the height of any of the two layers (1 or 2 respectively) over the sum of the two layers. The Drude model used in previous chapter for InAs is used for its permittivity, and AlAs refractive index is set to be 2.82. Computing this equation at various InAs doping level, we get the effective material permittivity as shown in Figure 5-12 (a & c), the plain doped InAs permittivity is shown to its side for reference, Figure 5-12 (b & d).

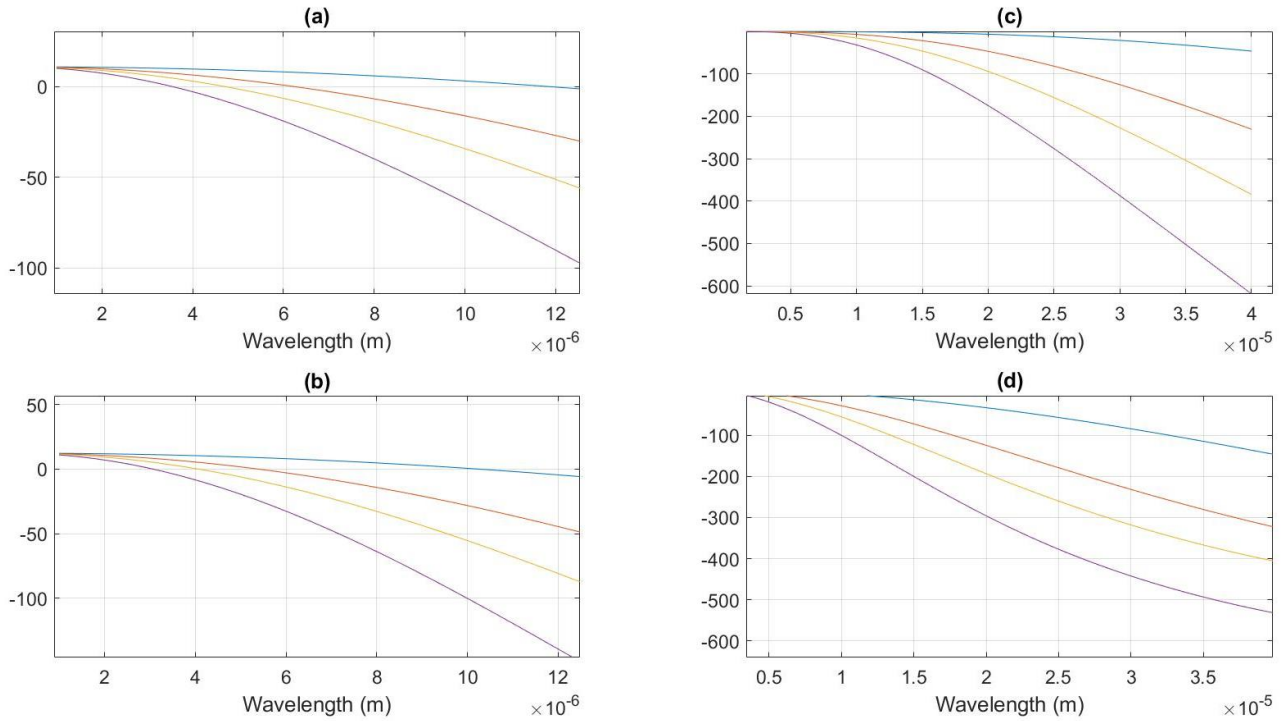


Figure 5-12, (a & c) shows the effective media permittivity real and imaginary parts respectively at different doping levels, and (b & d) shows the plain doped InAs permittivity real and imaginary parts respectively at different doping levels.

As can be seen from Figure 5-12, (a & c) shows the effective media permittivity real and imaginary parts respectively at different doping levels, and (b & d) shows the plain doped InAs permittivity real and imaginary parts respectively, the effective media permittivity has zero crossings at higher wavelength values, as compared to plain doped InAs, which means higher plasma frequency at the same charge concentration level. Also, the imaginary part is lower, which reflects the fact the effective material has an overall lower conductivity due to the presence of the dielectric.

Second, based on the new effective media permittivity, new dispersion curves for the hybrid plasmonic waveguide is computed, *Figure 5-13, dispersion curves of the hybrid plasmonic modes, at four different doping levels, real (upper plot) and imaginary (Lower plot) parts.* Also, Dispersion curves for the optical waveguide (*Figure 5-10*) is also computed, with AIAs model refractive index is set to 2.82, GaAs-Palik model used from the library of Lumerical simulator, and according to [25], the refractive index of  $Al_{0.9}GaAs$  is 2.85.



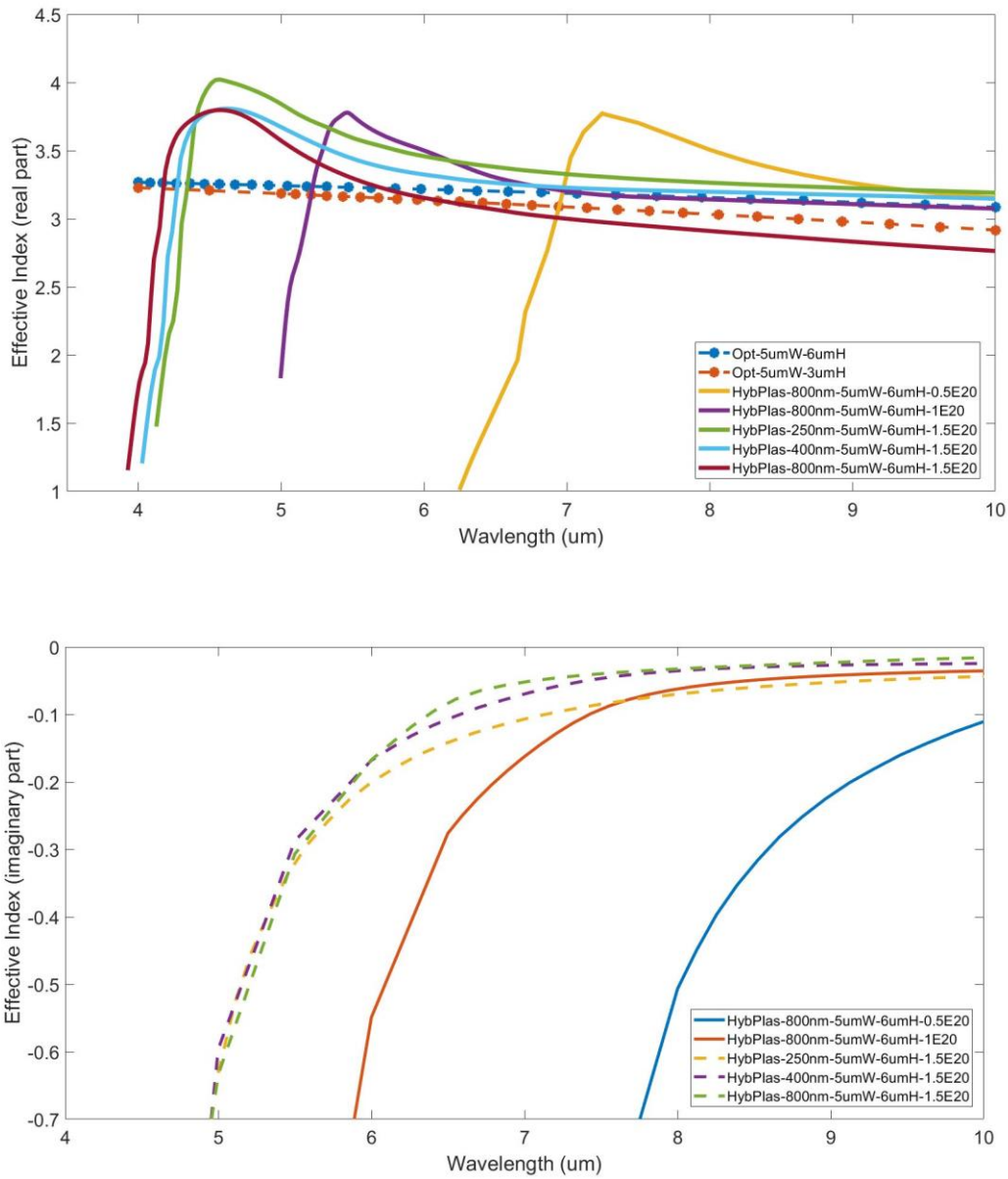


Figure 5-13, dispersion curves of the hybrid plasmonic modes, at four different doping levels, real (upper plot) and imaginary (Lower plot) parts. Also, dispersion curves of the optical modes are presented.

Figure 5-13 shows two sets of curves, first the hybrid plasmonic dispersion curves are computed versus two main parameters, the core height, and the InAs charge concentration. It was found that the height

has little effect on the hybrid plasmonic dispersion behavior. Second, the optical modes dispersion curves are computed at two different heights.

The modulator concept is based on absorption of the optical power coupled from the optical waveguide to the hybrid plasmonic waveguide. Consequently, for optimum modulator performance, both coupling and hybrid plasmonic modulator losses should be optimized. In other words, best momentum matching leads to best coupling, but due to low relative hybrid plasmonic mode losses at the point of best momentum matching, overall modulator absorption is not necessarily the best. Hence, both momentum matching and hybrid plasmonic mode losses are optimized to give us the optimum overall modulator response.

## 5.5 FDTD SIMULATIONS

The device is electromagnetically completely modeled using Lumerical Finite Difference Time Domain (FDTD). All FDTD simulations is done on Lumerical FDTD, no part of the structure has less than twenty mesh elements, and usually most of the structure has much more than this limit. Meshing convergence test was also done to ensure that meshing is not a parameter that affects the results. All the boundary conditions were chosen to be phase matched layer, and they were optimized to ensure no reflections from the boundaries. The same previously mentioned Material parameters (in the Mode Analysis section) are used.

Figure 5-14 shows the wide band transmission response of the modulator for a 40 um modulator. The modulator response is divided into two parts. First, the normal operation is the wavelength range where normal coupling from the optical waveguide to the plasmonic waveguide occurs, and then the field dies in the plasmonic mode. The minimum of the curve differs with the voltage (charge concentration), as at lower voltage levels, higher wavelength ranges is absorbed in the plasmonic waveguide, and vice versa. Second, the resonance operation, this part shows the significant results. It was found that, due to the presence of the superlattice, the plasmonic mode gets absorbed inside the superlattice at specific wavelengths, as shown in Figure 5-15, yielding very high extinction ratios.

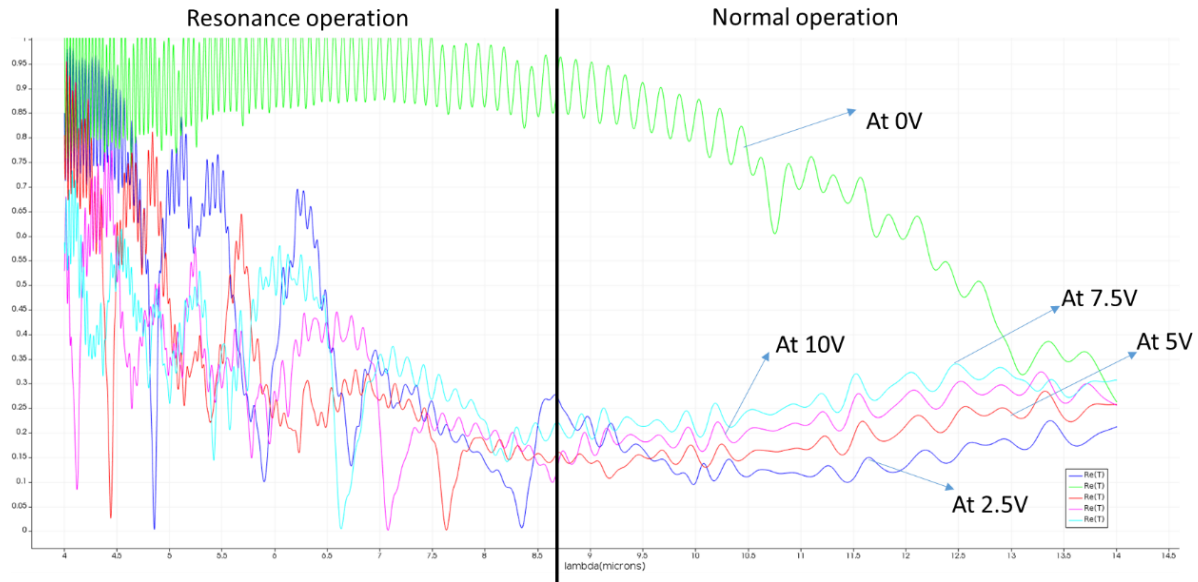


Figure 5-14, wide band transmission of the modulator. The modulator response is divided into two parts, the first part is called the resonance regime, the second part is called the normal regime.

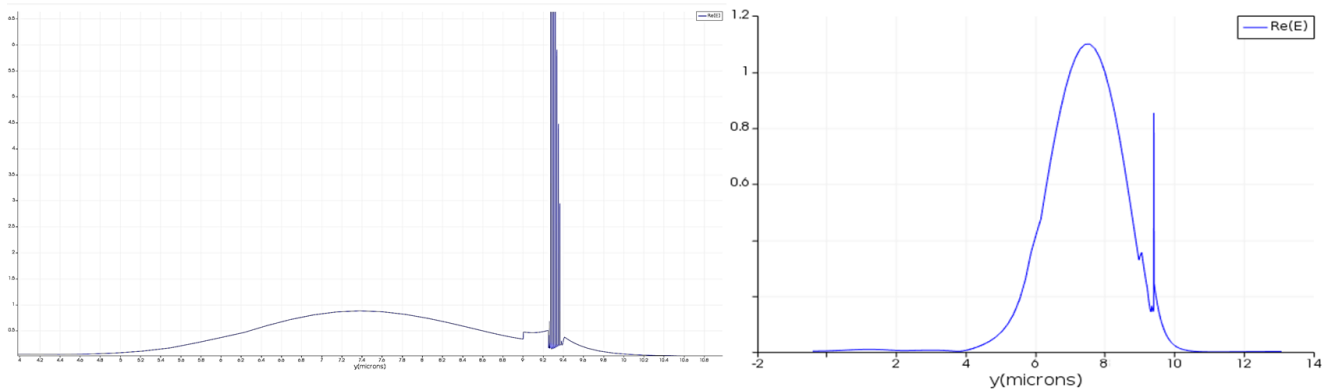


Figure 5-15, Modal shape at resonance, at wavelength equal to 4.85 microns in the Off state (to the left), and On State (to the right).

Figure 5-16 Shows the On and Off operations at wavelength equal to 4.85 microns. The transmission at this wavelength is shown in Figure 5-17, where the extinction ratio is 27 dB, and the insertion loss is 1.2 dB. The same response can be shown at wavelengths 6.6 microns in Figure 5-18, where the extinction ratio is equal to 16.7 dB, and the insertion loss is 1.55 dB.

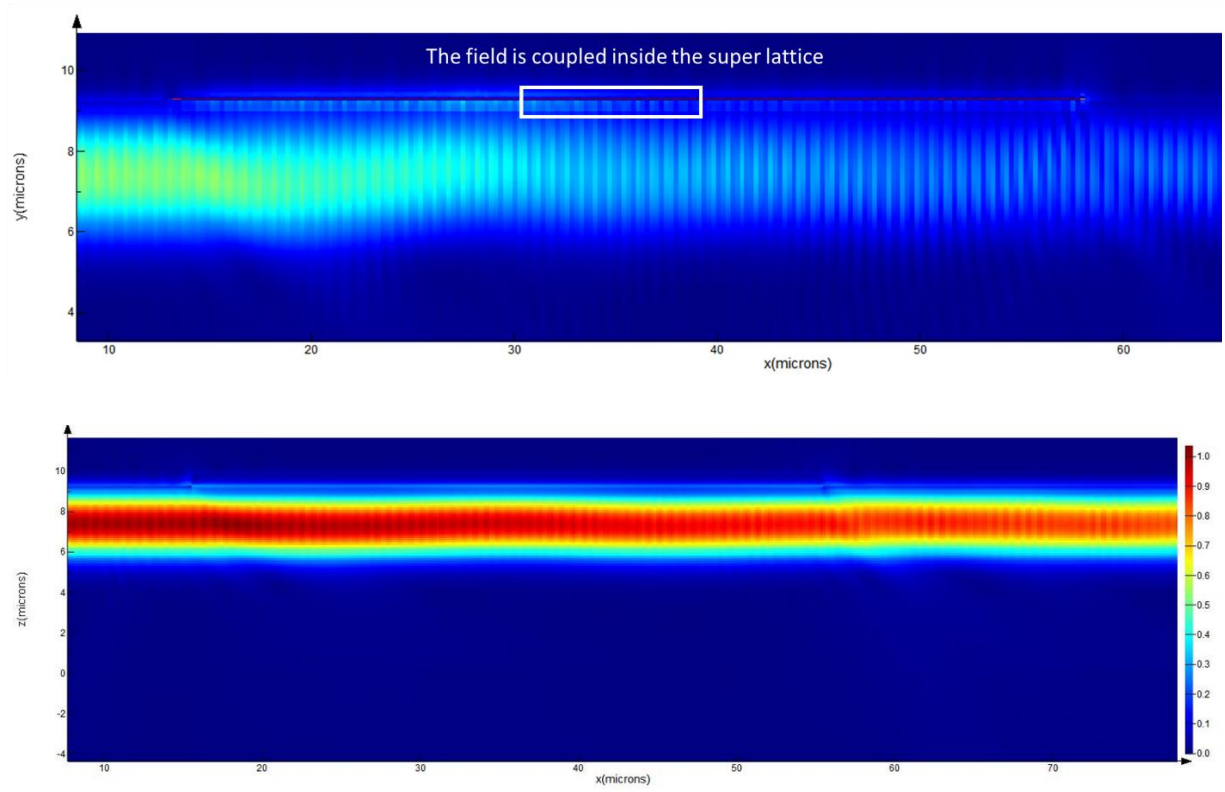


Figure 5-16, The upper figure shows the modulator off state, while the lower figure shows the modulator on state.

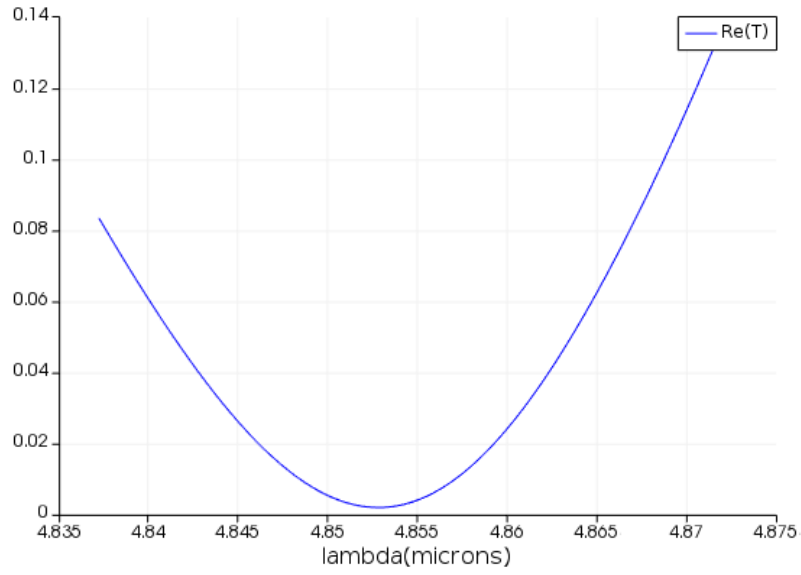


Figure 5-17, transmission at wavelength equal to 4.85 at 2.5V.

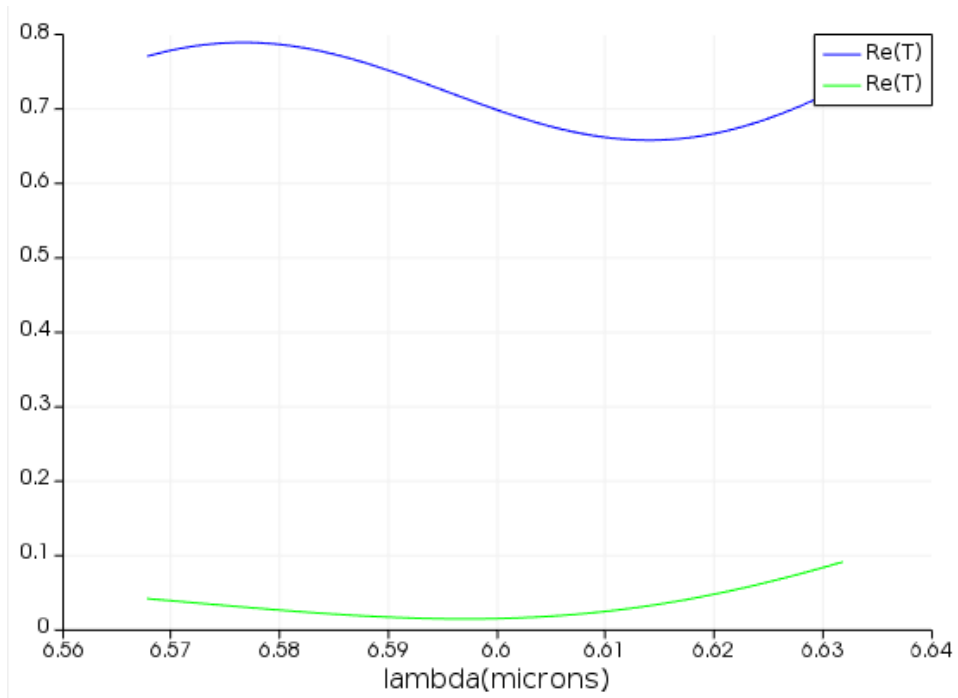


Figure 5-18, transmission at wavelength equal to 6.6 at 7.5V.

## 5.6 CONCLUSION

An electro-absorption modulator based on a hybrid plasmonic waveguide formed of doped InAs/AlAs/GaAs fed from GaAs/AlGaAs platform optical waveguide. The device is modeled and optimized, for on-chip optical sensor circuits in the mid-infrared region. The modulation happens by accumulating carriers electrically, and hence controlling the field coupling between the optical mode and the hybrid plasmonic lossy waveguide. The device showed an extinction ratio of 27 dB at 40  $\mu\text{m}$  length, and 1.2 dB of insertion loss. The small device footprint predicts a low energy consumption.

## REFERENCES:

- [1] S. Law, V. Podolskiy, and D. Wasserman, "Towards nano-scale photonics with micro-scale photons: the opportunities and challenges of mid-infrared plasmonics," *Nanophotonics*, vol. 2, 2013.
- [2] Soref, R. Mid-infrared photonics in silicon and germanium. *Nature Photon* **4**, 495–497 (2010). <https://doi.org/10.1038/nphoton.2010.171>
- [3] R. Soref, "Enabling 2  $\mu\text{m}$  communications," *Nat. Photonics* 9(6), 358–359 (2015).
- [4] G. Z. Mashanovich, M. Nedeljkovic, J. Soler-Penades, Z. Qu, W. Cao, A. Osman, Y. Wu, C. J. Stirling, Y. Qi, Y.X. Cheng, L. Reid, C. G. Littlejohns, J. Kang, Z. Zhao, M. Takenaka, T. Li, Z. Zhou, F. Y. Gardes, D. J. Thomson, and G. T. Reed, "Group IV mid-infrared photonics [Invited]," *Opt. Mater.*
- [5] Yao, Y., Hoffman, A. & Gmachl, C. Mid-infrared quantum cascade lasers. *Nature Photon* **6**, 432–439 (2012). <https://doi.org/10.1038/nphoton.2012.143>
- [6] Markus Sieger and Boris Mizaikoff *Analytical Chemistry* 2016 88 (11), 5562-5573 DOI: 10.1021/acs.analchem.5b04143
- [7] Popa, Daniel; Udrea, Florin. 2019. "Towards Integrated Mid-Infrared Gas Sensors" *Sensors* 19, no. 9: 2076. <https://doi.org/10.3390/s19092076>

- [8] Peter Werle, Franz Slemr, Karl Maurer, Robert Kormann, Robert Mücke, Bernd Jänker, Near- and mid-infrared laser-optical sensors for gas analysis, *Optics and Lasers in Engineering*, Volume 37, Issues 2–3, 2002, Pages 101-114, ISSN 0143-8166, [https://doi.org/10.1016/S0143-8166\(01\)00092-6](https://doi.org/10.1016/S0143-8166(01)00092-6).
- [9] Mizaikoff, B. "Infrared optical sensors for water quality monitoring." *Water Science and Technology* 47, no. 2 (2003): 35-42.
- [10] Razeghi, Manijeh, and Binh-Minh Nguyen. "Advances in mid-infrared detection and imaging: a key issues review." *Reports on Progress in Physics* 77, no. 8 (2014): 082401.
- [11] T. R. Harris, "Optical properties of Si, Ge, GaAs, GaSb, InAs, and InP at elevated temperatures," Master, Air Force Institute of Technology, 2010.
- [12] A. G. Milnes and A. Y. Polyakov, "Indium arsenide: a semiconductor for high speed and electro-optical devices," *Materials Science and Engineering: B*, vol. 18, pp. 237-259, 1993/04/15 1993.
- [13] R. Gamal, Y. Ismail, and M. A. Swillam, "Silicon Waveguides at the Mid-Infrared Range," *Journal of Lightwave Technology*, vol. 33, pp. 3207 - 3214, 2015.
- [14] D. Li and C. Z. Ning, "All-semiconductor active plasmonic system in mid-infrared wavelengths," *Optics Express*, vol. 19, pp. 14594-14603, 2011/07/18 2011.
- [15] N. V. Zotova, N. D. Il'inskaya, S. A. Karandashev, B. A. Matveev, M. A. Remennyi, and N. M. Stus', "Sources of spontaneous emission based on indium arsenide," *Semiconductors (Translation of Fizika i Tekhnika Poluprovodnikov (Sankt-Peterburg))*, vol. 42, pp. 625-641, 2008.
- [16] M. Nedeljkovic *et al.*, "Mid-Infrared Thermo-Optic Modulators in Sol," in *IEEE Photonics Technology Letters*, vol. 26, no. 13, pp. 1352-1355, July 1, 2014, doi: 10.1109/LPT.2014.2323702.
- [17] M. Nedeljkovic, S. Stanković, C. Mitchell, A. Z. Khokhar, S. Reynolds, D. J. Thomson, F. Y. Gardes, C. Littlejohns, G. T. Reed, and G. Z. Mashanovich, "Mid-infrared thermo-optic modulators in SOI," *IEEE Photonics Technol. Lett.* 26(13), 1352–1355 (2014).
- [18] J. Chiles and S. Fathpour, "Mid-infrared integrated waveguide modulators based on silicon-on-lithium-niobate photonics," *Optica* 1(5), 350–355 (2014).
- [19] M. A. Van Camp, S. Assefa, D. M. Gill, T. Barwicz, S. M. Shank, P. M. Rice, T. Topuria, and W. M. J. Green, "Demonstration of electrooptic modulation at 2165nm using a silicon Mach-Zehnder interferometer," *Opt. Express* 20(27), 28009–28016 (2012).

- [20] J. Kang, M. Takenaka, and S. Takagi, "Novel Ge waveguide platform on Ge-on-insulator wafer for mid-infrared photonic integrated circuits," *Opt. Express* 24(11), 11855–11864 (2016).
- [21] Oulton, R. F., et al. "A Hybrid Plasmonic Waveguide for Subwavelength Confinement and Long-Range Propagation." *Nature Photonics*, vol. 2, no. 8, 2008, pp. 496–500., doi:10.1038/nphoton.2008.131.
- [22] Charlton, Christy, Marcella Giovannini, Jérôme Faist, and Boris Mizaikoff. "Fabrication and characterization of molecular beam epitaxy grown thin-film GaAs waveguides for mid-infrared evanescent field chemical sensing." *Analytical chemistry* 78, no. 12 (2006): 4224-4227.
- [23] Schädle, Thomas, and Boris Mizaikoff. "Mid-infrared waveguides: a perspective." *Applied spectroscopy* 70, no. 10 (2016): 1625-1638.
- [24] Sieger, Markus, Julian Haas, Michael Jetter, Peter Michler, Matthias Godejohann, and Boris Mizaikoff. "Mid-infrared spectroscopy platform based on GaAs/AlGaAs thin-film waveguides and quantum cascade lasers." *Analytical chemistry* 88, no. 5 (2016): 2558-2562.
- [25] S. Adachi. Optical dispersion relations for GaP, GaAs, GaSb, InP, InAs, InSb,  $\text{Al}_x\text{Ga}_{1-x}\text{As}$ , and  $\text{In}_{1-x}\text{Ga}_x\text{As}_y\text{P}_{1-y}$ , [J. Appl. Phys. 66, 6030-6040 \(1989\)](#)
- [26] Kittel, C., Introduction to Solid State Physics, 6th Ed., New York:John Wiley, 1986, p. 185.
- [27] P. Lalanne and D. Lemercier-lalanne, *J. Mod. Opt.* 43, 2063 (1996).

## Chapter 6: CONCLUSION

On chip optical interconnects are becoming a must for the continuing increasing need for higher data rates, and higher processing capabilities. Also, on-chip optical sensing can extensively help health care systems in fast and reliable diagnosis. For these two purposes, nanoscale optical modulators with high modulation depth, and low power consumption is of high need. More exploration for the interdisciplinary physics of the light matter interaction is of needed to reach this goal.



In this thesis, we designed two optical modulators. The first targets the optical interconnects application in the infrared region at  $1.55\mu\text{m}$ , and it is based on silicon on insulator technology. The second targets on chip optical sensor photonic circuits in the mid-infrared region, and it is based on III-V semiconductors technology. For the purpose of building the mid-infrared modulator, a complete hybrid plasmonic waveguide was built and analyzed.

First, an organic plasmonic electro-refractive modulator based on Mach-Zehnder interferometer was designed. The orthogonal junction coupling technique between optical waveguides, and the highly confining metal insulator metal plasmonic waveguides is utilized to couple wideband power streams instantly without the need for length taper structures. The device is optimized to work at the optical communication wavelength  $1.55\mu\text{m}$  wavelength. For a footprint of  $0.6\mu\text{m} \times 4.7\mu\text{m}$ , extinction ratio of 15.8 dB and insertion loss of 3.38 dB at 10 volts was achieved in the 3D simulations. The product of voltage and length of the modulator is  $47\text{ V}\mu\text{m}$ . Orthogonal junction coupling scheme enhances the modulator footprint, and consequently lowers plasmonic losses in the on state of the modulator, meaning lower insertion loss. It also allowed for high field interaction at the modulator's output port, meaning a higher value of extinction ratio, while keeping the voltage length product approximately the same.

Next, doped semiconductors were used as an alternative to metals, the doping enables us to control the plasma frequency of the semiconductor to the wavelength of interest, in our case the mid infrared region. Using this feature, a hybrid plasmonic waveguide was designed and analyzed. III-V semiconductor media are used, to take advantage of the fact that, quantum cascade laser sources, the most efficient and promising laser sources in this wavelength range is built using the III-V technology. Dispersion curves were calculated for the waveguide vs doping, and dimensions, showing how to utilize this waveguide for a particular application. Positive, negative dispersions, and a point of zero phase velocity were found, and we were able to control the dispersion curve features through doping. The negative dispersion properties of this waveguide will enable it to enter a new category of applications. From the fabrication point of view, this device is simple as it consists of three thin films over a GaAs substrate.

Finally, an electro-absorption modulator in the midinfrared region, targeting the on chip optical sensor circuits is was designed. The modulator is based on the hybrid plasmonic waveguide formed of doped InAs/AlAs/GaAs that is presented in chapter 4. The modulator is fed from GaAs/AlGaAs platform optical

waveguides, which is compatible with quantum cascade lasers, the light sources mainly used in this wavelength region. Modulation occurs by electrically depleting the carriers from the InAs, consequently controlling the field coupling from the optical mode to the hybrid plasmonic waveguide. The device showed an extinction ratio of 15 dB at 40  $\mu\text{m}$  length, and 2 dB of insertion loss. The small device footprint predicts a much lower energy consumption.

The connecting theme between the three pieces of work presented above, is to further understand light matter interaction to build smaller and more efficient optical modulators.

## BIBLIOGRAPHY

### 6.1

- [16] Gramotnev DK, Bozhevolnyi SI . Plasmonics beyond the diffraction limit . *Nat Photonics* 2010 ; **4** : 83 – 91.
- [17] Zia R, Schuller JA, Chandran A, Brongersma ML . Plasmonics: the next chip-scale technology . *Mater Today* 2006 ; **9** : 20 – 27.

- [18] Barnes WL, Dereux A, Ebbesen TW . Surface plasmon subwavelength optics . *Nature* 2003 ; **424** : 824 – 830.
- [19] Maier SA, Kik PG, Atwater HA, Meltzer S, Harel E *et al* . Local detection of electromagnetic energy transport below the diffraction limit in metal nanoparticle plasmon waveguides . *Nat Mater* 2003 ; **2** : 229 – 232.
- [20] Quinten M, Leitner A, Krenn JR, Aussenegg FR . Electromagnetic energy transport via linear chains of silver nanoparticles . *Opt Lett* 1998 ; **23** : 1331 – 1333.
- [21] Alu A, Engheta N . Effect of small random disorders and imperfections on the performance of arrays of plasmonic nanoparticles . *New J Phys* 2010 ; **12** : 013015.
- [22] Liu N, Mukherjee S, Bao K, Li Y, Brown LV *et al* . Manipulating magnetic plasmon propagation in metallic nanocluster networks . *ACS Nano* 2012 ; **6** : 5482 – 5488.
- [23] Economou EN . Surface plasmons in thin films . *Phys Rev* 1969 ; **182** : 539 – 554.
- [24] Lopez-Tejiera F, Rodrigo SG, Martin-Moreno L, Garcia-Vidal FJ, Devaux E *et al* . Efficient unidirectional nanoslit couplers for surface plasmons . *Nat Phys* 2007 ; **3** : 324 – 328.
- [25] Bozhevolnyi SI, Volkov VS, Devaux E, Ebbesen TW . Channel plasmon-polariton guiding by subwavelength metal grooves . *Phys Rev Lett* 2005 ; **95** : 046802.
- [26] Sanders AW, Routenberg DA, Wiley BJ, Xia YN, Dufresne ER *et al* . Observation of plasmon propagation, redirection, and fan-out in silver nanowires . *Nano Lett* 2006 ; **6** : 1822 – 1826.
- [27] Ditlbacher H, Hohenau A, Wagner D, Kreibitz U, Rogers M *et al* . Silver nanowires as surface plasmon resonators . *Phys Rev Lett* 2005 ; **95** : 257403.
- [28] Fang YR, Wei H, Hao F, Nordlander P, Xu HX . Remote-excitation surface-enhanced Raman scattering using propagating Ag nanowire plasmons . *Nano Lett* 2009 ; **9** : 2049 – 2053.
- [29] Boardman AD, Aers GC, Teshima R . Retarded edge modes of a parabolic wedge . *Phys Rev B* 1981 ; **24** : 5703 – 5712.
- [30] Han ZH, Bozhevolnyi SI . Radiation guiding with surface plasmon polaritons . *Rep Prog Phys* 2013 ; **76** : 016402.

- [1] Kondo J et al 2005 High-speed and low-driving-voltage thin-sheet X-cut LiNbO<sub>3</sub> modulator with laminated low-dielectric-constant adhesive IEEE Photon. Technol. Lett. 17 2077–9.
- [2] Reed, G. T., and Weiss, B. L., Electron. Lett. (1987) 23, 424.
- [3] Pavesi, L., et al., Towards the First Silicon Laser, NATO Science Series, Kluwer.
- [4] Academic Publications, Dordrecht, (2003).
- [5] Poleman, A., et al., J. Appl. Phys. (1995) 77 (3), 1256.
- [6] D. J. Albares, R. A. Soref, "Silicon-On-Sapphire Waveguides," Proc. SPIE 0704, Integrated Optical Circuit Engineering IV, (10 March 1987); <https://doi.org/10.1117/12.937191>
- [7] R. A. Soref, J. Schmidtchen and K. Petermann, "Large single-mode rib waveguides in GeSi-Si and Si-on-SiO<sub>2</sub>," in IEEE Journal of Quantum Electronics, vol. 27, no. 8, pp. 1971-1974, Aug. 1991, doi: 10.1109/3.83406.
- [8] B. L. Weiss, G. T. Reed, S. K. Toh, R. A. Soref and F. Namavar, "Optical waveguides in SIMOX structures," in IEEE Photonics Technology Letters, vol. 3, no. 1, pp. 19-21, Jan. 1991, doi: 10.1109/68.68035.
- [9] G.T. Reed, Li Jinhua, C.K. Tang, Lin Chenglu, P.L.F. Hemment, A.G. Rickman, Silicon on insulator optical waveguides formed by direct wafer bonding, Materials Science and Engineering: B, Volume 15, Issue 2, 1992, Pages 156-159, ISSN 0921-5107, [https://doi.org/10.1016/0921-5107\(92\)90048-E](https://doi.org/10.1016/0921-5107(92)90048-E).
- [10] Richard A. Soref and Brian R. Bennett "Kramers-Kronig Analysis Of Electro-Optical Switching In Silicon", Proc. SPIE 0704, Integrated Optical Circuit Engineering IV, (10 March 1987); <https://doi.org/10.1117/12.937193>.
- [11] U. Fischer, B. Schuppert and K. Petermann, "Integrated optical switches in silicon based on SiGe-waveguides," in IEEE Photonics Technology Letters, vol. 5, no. 7, pp. 785-787, July 1993, doi: 10.1109/68.229806.
- [12] A. Cutolo, M. Iodice, P. Spirito and L. Zeni, "Silicon electro-optic modulator based on a three terminal device integrated in a low-loss single-mode SOI waveguide," in Journal of Lightwave Technology, vol. 15, no. 3, pp. 505-518, March 1997, doi: 10.1109/50.557567.

- [13] C. K. Tang, G. T. Reed, A. J. Walton and A. G. Rickman, "Low-loss, single-model optical phase modulator in SIMOX material," in *Journal of Lightwave Technology*, vol. 12, no. 8, pp. 1394-1400, Aug. 1994, doi: 10.1109/50.317527.
- [14] Tang, C. K., et al., *Mat. Res. Soc. Symp. Proc.* (1993) 298, 247.
- [15] Tang, C. K., and Reed, G. T., "Highly efficient optical phase modulator in SOI waveguides" *Electron. Lett.* (1995) 31 (6), 451.
- [16] Liu, A., Jones, R., Liao, L. et al. A high-speed silicon optical modulator based on a metal–oxide–semiconductor capacitor. *Nature* 427, 615–618 (2004). <https://doi.org/10.1038/nature02310>
- [17] Soref, R. A., and Bennett, B. R., *Proc. SPIE* (1986) 704, 32.
- [18] Barnes WL, Dereux A, Ebbesen TW . Surface plasmon subwavelength optics . *Nature* 2003 ; **424** : 824 – 830.
- [19] Maier SA, Kik PG, Atwater HA, Meltzer S, Harel E *et al* . Local detection of electromagnetic energy transport below the diffraction limit in metal nanoparticle plasmon waveguides . *Nat Mater* 2003 ; **2** : 229 – 232.
- [20] Quinten M, Leitner A, Krenn JR, Aussenegg FR . Electromagnetic energy transport via linear chains of silver nanoparticles . *Opt Lett* 1998 ; **23** : 1331 – 1333.
- [21] Gramotnev DK, Bozhevolnyi SI . Plasmonics beyond the diffraction limit . *Nat Photonics* 2010 ; **4** : 83 – 91.
- [22] Chen JJ, Sun CW, Hu XY . Nanoscale all-optical devices based on surface plasmon polaritons . *Chinese Sci Bull* 2014 ; **59** : 2661 – 2665.
- [23] Han ZH, Bozhevolnyi SI . Radiation guiding with surface plasmon polaritons . *Rep Prog Phys* 2013 ; **76** : 016402.
- [24] Zia R, Schuller JA, Chandran A, Brongersma ML . Plasmonics: the next chip-scale technology . *Mater Today* 2006 ; **9** : 20 – 27.
- [25] Liu N, Mukherjee S, Bao K, Li Y, Brown LV *et al* . Manipulating magnetic plasmon propagation in metallic nanocluster networks . *ACS Nano* 2012 ; **6** : 5482 – 5488.
- [26] Chang DE, Sorensen AS, Hemmer PR, Lukin MD . Strong coupling of single emitters to surface plasmons . *Phys Rev B* 2007 ; **76** : 035420.
- [27] Alu A, Engheta N . Effect of small random disorders and imperfections on the performance of arrays of plasmonic nanoparticles . *New J Phys* 2010 ; **12** : 013015.

- [28] M. Nedeljkovic, S. Stanković, C. Mitchell, A. Z. Khokhar, S. Reynolds, D. J. Thomson, F. Y. Gardes, C. Littlejohns, G. T. Reed, and G. Z. Mashanovich, "Mid-infrared thermo-optic modulators in SOI," *IEEE Photonics Technol. Lett.* 26(13), 1352–1355 (2014).
- [29] J. Chiles and S. Fathpour, "Mid-infrared integrated waveguide modulators based on silicon-on-lithium-niobate photonics," *Optica* 1(5), 350–355 (2014).
- [30] R. Soref, "Enabling 2  $\mu\text{m}$  communications," *Nat. Photonics* 9(6), 358–359 (2015).
- [31] G. Z. Mashanovich, M. Nedeljkovic, J. Soler-Penades, Z. Qu, W. Cao, A. Osman, Y. Wu, C. J. Stirling, Y. Qi, Y.X. Cheng, L. Reid, C. G. Littlejohns, J. Kang, Z. Zhao, M. Takenaka, T. Li, Z. Zhou, F. Y. Gardes, D. J. Thomson, and G. T. Reed, "Group IV mid-infrared photonics [Invited]," *Opt. Mater.*
- [32] M. Nedeljkovic *et al.*, "Mid-Infrared Thermo-Optic Modulators in Sol," in *IEEE Photonics Technology Letters*, vol. 26, no. 13, pp. 1352-1355, July1, 2014, doi: 10.1109/LPT.2014.2323702.
- [33] J. Kang, M. Takenaka, and S. Takagi, "Novel Ge waveguide platform on Ge-on-insulator wafer for mid-infrared photonic integrated circuits," *Opt. Express* 24(11), 11855–11864 (2016).
- [34] M. A. Van Camp, S. Assefa, D. M. Gill, T. Barwicz, S. M. Shank, P. M. Rice, T. Topuria, and W. M. J. Green, "Demonstration of electrooptic modulation at 2165nm using a silicon Mach-Zehnder interferometer," *Opt. Express* 20(27), 28009–28016 (2012).
- [35] D. J. Thomson, L. Shen, J. J. Ackert, E. Huante-Ceron, A. P. Knights, M. Nedeljkovic, A. C. Peacock, and G. Z. Mashanovich, "Optical detection and modulation at 2 $\mu\text{m}$ -2.5 $\mu\text{m}$  in silicon," *Opt. Express* 22(9), 10825–10830 (2014).
- [36] M. Nedeljkovic, R. Soref, and G. Z. Mashanovich, "Free-carrier electrorefraction and electroabsorption modulation predictions for silicon over the 1-14- $\mu\text{m}$  infrared wavelength range," *IEEE Photonics J.* 3(6), 1171–1180 (2011).
- [37] M. Nedeljkovic, R. Soref, and G. Z. Mashanovich, "Predictions of free-carrier electroabsorption and electrorefraction in germanium," *IEEE Photonics J.* 7(3), 1–14 (2015). Vol 8, 2276-2286 (2018).
- [38] Vol. 8, No. 8 | 1 Aug 2018 | OPTICAL MATERIALS EXPRESS 2282.
- [39] Semiconductor Industry Association, The International Technology Roadmap for Semiconductors, 2013. [Online].
- [40] Available: <http://www.itrs2.net/2013-itrs.html>
- [41] Semiconductor Industry Association, The International Technology Roadmap for Semiconductors, 2015. [Online].

- [42] Available: <http://www.itrs2.net/2013-itrs.html>
- [43] D. Korn *et al.*, "Silicon-organic hybrid (SOH) IQ modulator using the linear electro-optic effect for transmitting 16QAM at 112 Gbit/s," *Opt. Exp.*, vol. 21, pp. 13219–13227, 2013.
- [44] H. Xu *et al.*, "High-speed silicon modulator with band equalization," *Opt. Lett.*, vol. 39, pp. 4839–4842, 2014.
- a. Dhiman, "Silicon photonics: A review," *IOSR J. Appl. Phys.*, vol. 3, pp. 67–79, 2013.
- [45] G. T. Reed, G. Mashanovich, F. Y. Gardes, and D. J. Thomson, "Silicon optical modulators," *Nature Photon.*, vol. 4, pp. 518–526, 2010.
- [46] D. K. Gramotnev and S. I. Bozhevolnyi, "Plasmonics beyond the diffraction limit," *Nature Photon.*, vol. 4, pp. 83–91, 2010.
- [47] Z. Ma, Z. Li, K. Liu, C. Ye, and V. J. Sorger, "Indium-tin-oxide for high-performance electro-optic modulation," *Nanophotonics*, vol. 4, pp. 198–213, 2015.
- [48] X. Yang *et al.*, "Hybrid photonic Plasmonic crystal nanocavities," *ACS Nano*, vol. 5, pp. 2831–2838, 2011.
- [49] Y.-F. Xiao *et al.*, "Strongly enhanced light-matter interaction in a hybrid photonic-plasmonic resonator," *Phys. Rev. A*, vol. 85, 2012, Art. no. 031805.
- [50] C. Ciminelli, D. Conteduca, F. Dell'Olio, and M. N. Armenise, "Design of an optical trapping device based on an ultra-high Q/V resonant structure," *IEEE Photon. J.*, vol. 6, no. 6, Dec. 2014, Art. no. 0600916.
- [51] D. Conteduca *et al.*, "Rigorous design of an ultra-high Q/V photonic/plasmonic cavity to be used in biosensing applications," *Opt. Laser Technol.*, vol. 77, pp. 151–161, 2016.
- a. O. Zaki, N. H. Fouad, D. C. Zografopoulos, R. Beccherelli, and M. A. Swillam, "Low-power compact hybrid plasmonic double-microring electro-optical modulator," *Proc. SPIE*, vol. 9744, 2016, Art. no. 97441K.
  - b. Sun *et al.*, "Single-chip microprocessor that communicates directly using light," *Nature*, vol. 528, pp. 534–538, 2015.
  - c. Guha, A. Gondarenko, and M. Lipson, "Minimizing temperature sensitivity of silicon Mach-Zehnder interferometers,"
- [52] *Opt. Exp.*, vol. 18, pp. 1879–1887, 2010.

- [53]S. Zhu, G. Q. Lo, and D. L. Kwong, "Electro-absorption modulation in horizontal metal-insulator-silicon-insulator-metal nanoplasmonic slot waveguides," *Appl. Phys. Lett.*, vol. 99, 2011, Art. no. 151114.
- [54]A. O. Zaki, K. Kirah, and M.A. Swillam, "Hybrid plasmonic electro-optical modulator," *Appl. Phys. A*, vol. 122, pp. 473–479, 2016.
- [55]M. Liu *et al.*, "A graphene-based broadband optical modulator," *Nature*, vol. 474, pp. 64–67, 2011.
- [56]J.-S. Shin and J. T. Kim, "Broadband silicon optical modulator using a graphene-integrated hybrid plasmonic waveguide,"
- [57]*Nanotechnology*, vol. 26, 2015, Art. no. 365201.
- [58]V. J. Sorger, N. D. Lanzillotti-Kimura, R.-M. Ma, and X. Zhang, "Ultra-compact silicon nanophotonic modulator with broadband response," *Nanophotonics*, vol. 1, pp. 17–22, 2012.
- [59]V. E. Babicheva, "Ultra-compact plasmonic waveguide modulators," DTU FOTONIK, Dept. Photon. Eng., Tech. Univ. Denmark, Kongens Lyngby, Denmark, 2013.
- [60]M. Xu *et al.*, "Design of an electro-optic modulator based on a silicon-plasmonic hybrid phase shifter," *J. Lightw. Technol.*, vol. 31, no. 8, pp. 1170–1177, Apr. 2013.
- [61]K. F. MacDonald and N. I. Zheludev, "Theoretical investigation of silicon MOS-type plasmonic slot waveguide based MZI modulators," *Laser Photon. Rev.*, vol. 4, pp. 562–567, 2010.
- [62]C. Haffner *et al.*, "All-plasmonic Mach–Zehnder modulator enabling optical high-speed communication at the microscale," *Nature Photon.*, vol. 9, pp. 525–528, 2015.
- [63]C. Lin, H. M. Wong, B. Lau, M. A. Swillam, and A. S. Helmy, "Efficient broadband energy transfer via momentum matching at hybrid junctions of guided-waves," *Appl. Phys. Lett.*, vol. 101, 2012, Art. no.123115.
- [64]B. Lau, M. A. Swillam, and A. S. Helmy, "Hybrid orthogonal junctions: Wideband plasmonic slot-silicon waveguide couplers," *Opt. Exp.*, vol. 18, pp. 27048–27059, 2010.
- [65]Lumerical Solutions, Inc., Vancouver, BC, Canada. 2003. [Online]. Available: <http://www.lumerical.com/tcad-products/fdtd/>
- [66]P. B. Johnson and R. W. Christy, "Optical constants of noble metal," *Phys. Rev. B*, vol. 6, no. 12, pp. 4370–4379, 1973
- [67]J. Iverson *et al.*, "Electro-optic Pockels cell voltage sensors for accelerator diagnostics," College Eng., Montana State Univ., Bozeman, MT, Canada, 2004.



- [68]S. Michel, J. Zyss, I. Ledoux-Rak, and C. T. Nguyen, "High-performance electro-optic modulators realized with a commercial side-chain DR1-PMMA electro-optic copolymer," in *Proc. SPIE, Int. Soc. Opt. Photon.*, 2010, Art. no. 75990I.
- [69]D. A. B. Miller, "Device requirements for optical interconnects to silicon chips," *Proc. IEEE*, vol. 97, no. 7, pp. 1166–1185, Jul. 2009

- [70] Plasmonic waveguides in Mid infra-red using silicon-insulator-silicon. SPIE OPTO: International Society for Optics and Photonics; 2015.
- [71] Stanley R. Plasmonics in the mid-infrared. *Nature Photonics* 2012;6(7):409-411.
- [72] Law S, Podolskiy V, Wasserman D. Towards nano-scale photonics with micro-scale photons: the opportunities and challenges of mid-infrared plasmonics. *Nanophotonics* 2013;2(2):103-130.
- [73] Li D, Ning C. All-semiconductor active plasmonic system in mid-infrared wavelengths. *Optics express* 2011;19(15):14594-14603.
- [74] Yao Y, Hoffman AJ, Gmachl CF. Mid-infrared quantum cascade lasers. *Nature Photonics* 2012;6(7):432-439.
- [75] Palmer C, Stavrinou P, Whitehead M, Phillips C. Mid-infrared ( $\lambda \sim 2\text{--}6 \mu\text{m}$ ) measurements of the refractive indices of GaAs and AlAs. *Semiconductor science and technology* 2002;17(11):1189.
- [76] Law S, Adams D, Taylor A, Wasserman D. Mid-infrared designer metals. *Optics express* 2012;20(11):12155-12165.
- [77] Jain S, McGregor J, Roulston D. Band-gap narrowing in novel III-V semiconductors. *J Appl Phys* 1990;68(7):3747-3749.
- [78] Sotoodeh M, Khalid A, Rezazadeh A. Empirical low-field mobility model for III-V compounds applicable in device simulation codes. *J Appl Phys* 2000;87(6):2890-2900.
- [79] Popovic RS. Hall effect devices. : CRC Press; 2003.